SLIT AND RECEPTORS IN *D. melanogaster* HEART MORPHOGENESIS

FUNCTIONAL ANALYSIS OF THE ROLE OF SLIT AND ITS RECEPTORS DURING *D. melanogaster* HEART MORPHOGENESIS

by

KATERINA VASSILIEVA, B.Sc.

A Thesis
Submitted to the School of Graduate Studies
in Partial fulfillment of the Requirements
for the Degree
Master of Science

McMaster University

MASTER OF SCIENCE (2008) McMaster University
(Biology) Hamilton, Ontario

TITLE: Functional analysis of the role of Slit and its receptors during *D. melanogaster* heart morphogenesis.

AUTHOR: Katerina Vassilieva, B.Sc., University of Toronto

SUPERVISOR: J. Roger Jacobs, Ph.D., Professor, McMaster University

NUMBER OF PAGES: ix, 85

ABSTRACT

Proper formation of the heart is a critical developmental event which requires strict regulation of coordinated cardial cell adhesion, alignment, and migration. The simple, tube-like heart of the fruit fly, *Drosophila melanogaster,* has proven to be an attractive system in which to study the regulatory pathways which control cardiogenesis. This is mainly due to its strikingly similarity to the vertebrate heart during early embryogenesis. In addition, many genes identified in association with congenital heart disease in humans have homologues in *Drosophila*, suggesting that this model organism has great potential to contribute to cardiovascular research.

The extracellular matrix protein encoded by *slit* is a ligand for the receptors Robo, and Robo2 (*lea*). Recently, a third receptor for Slit has been identified as the heparin sulfate proteoglycan Syndecan. The main objective of this thesis was to use time lapse confocal imaging in order to develop further understanding of the mechanisms which result in heart assembly defects in *slit*, *robo,lea*, and *syndecan* mutants. We also aimed to gain a better understanding of the role of Syndecan within the Slit-Robo pathway and elucidate its relative contribution to development of the mature heart.

In mutants homozygous for *slit*, as well as mutants doubly heterozygous for *robo* and *lea*, cardial cell alignment, adhesion, and synchronized migration were disrupted. The heart phenotype of *syndecan* homozygous mutants was similar that of *slit* and *robo,lea*, however the migration speed of cells to the midline did not seem to be affected. Based on our findings, we hypothesize that Slit may have Syndecan-dependent and Syndecan-independent functions in the heart.

ACKNOWLEDGEMENTS

I would like to say thank you to my supervisor, Dr. Roger Jacobs for his continued support and guidance during the course of this project, and to Dr. Ana Campos for leading helpful discussions and teaching me to examine my work more critically. Thank you also to Tony Collins for his technical support with time lapse confocal equipment. Finally, thanks to members of the Jacobs lab, Mihaela Georgescu, Luz de Lourdes Vazquez Paz, Katherine Moyer, Leena Patel, and Noor Hossain, for making my lab experience memorable.

TABLE OF CONTENTS **PAGE**

LIST OF FIGURES **PAGE**

LIST OF ABBREVIATIONS

CHD	Congenital heart defect
CNS	Central nervous system
ECM	Extracellular matrix
EGF	Epidermal growth factor
lea	Gene encoding the receptor Robo2
GAL4	Galactosidase transgene with 4 binding sites
HS	Heparan sulfate
HSPG	Heparan sulfate proteoglycan
ILK	Integrin-linked kinase
lanA	Gene encoding the integrin ligand Laminin A
LRR	Leucine-rich repeat
prc	Gene encoding Pericardin, a component of the ECM
rhea	Gene encoding the intracellular messenger Talin
robo	Gene encoding the receptor Robo
scb	Gene encoding the αPS3 integrin
sdc^{97}	Gene encoding the receptor Syndecan
sli^{2}	Gene encoding the protein Slit
svp	Gene enocoding the protein Seven-up
tin	Gene encoding the homeodomain protein Tinman
tupGFP	Nuclear GFP marker under the control of the *tailup* gene
UAS	Upstream activating sequence
vkg	Gene encoding the integrin ligand Collagen IV
wb	Gene encoding the integrin ligand Lamini α1,2

CONTRIBUTIONS

Thank you to Randy Schulz at the University of Texas, Houston for providing us with the *tupGFP* stock, and Gerd Vorbrüggen at Gottingen, who provided us with sdc^{97}/CyO.

Chapter 1

Introduction

Proper formation of the heart is a critical developmental event during organogenesis which relies on coordinated cardial cell migration, adhesion, and alignment. Disruption in the regulation of any one of these critical processes in humans may result in congenital heart defects (CHDs), the most widely occurring birth defects (Hoffman, 1995; Hoffman, 2004). Currently, the cause of many CHDs remains elusive, due to a lack of understanding of the underlying genetic mechanisms affecting heart development. Animal models have been utilized to study the cellular and genetic events leading to appropriate heart formation. The fruit fly, *Drosophila melanogaster,* has proven to be an effective system in which to study cardiogenesis and the regulatory pathways that control this process. In addition, many genes identified in association with congenital heart disease in humans have homologues in *Drosophila*, suggesting that this model organism has great potential to contribute to cardiovascular research (Bier and Bodmer, 2004).

1.1 Structure and development of the *Drosophila* dorsal vessel

The simple, tube-like heart of *Drosophila* provides the simplest model for the study of cardiovascular development. The structure of the *Drosophila* embryonic heart or 'dorsal vessel' closely resembles a vertebrate capillary (Rugendorff et al., 1994). In humans, blood vessels are formed when a single layer of polarized endothelial cells is joined by junctions, forming a central lumen (Davis et al., 2000). A similar process takes

place in *Drosophila* to produce the lumen of the dorsal vessel, thus providing a model for vessel morphogenesis and lumen formation. Despite its rudimentary structure, there is a striking similarity between the early embryonic events of heart development in *Drosophila* and those of the vertebrate heart before looping morphogenesis (Chen and Fishmann, 2000). In fact, several studies have proposed that the cardiovascular system of *Drosophila* shares a phylogenetic relationship with the cardiovascular system of vertebrates (Harvey, 1996; Fishman and Olson, 1998; Hartenstein and Mandal, 2006). In both *Drosophila* and vertebrates, cardiac progenitor cells derived from laterally positioned mesoderm result in two bilaterally symmetrical strips of precardiac tissue that fuse at the midline (dorsally in *Drosophila*, ventrally in vertebrates), to form a linear tube (Bodmer, 1995).

The mature *Drosophila* heart consists of two rows of 52 contractile, myoendothelial cells called cardioblasts, which enclose a central lumen (Rugendorff et al. 1994). These cells are flanked laterally by non-contractile, unpolarized pericardial cells which are loosely attached to cardioblasts, and form the outer layer of the heart tube. Pericardial cells are involved in ultrafiltration and excretion of haemolymph (Crossley, 1985). The dorsal vessel runs in an anterior-posterior direction along the dorsal midline. The entire dorsal vessel spans from the second thoracic segment (T2) to the eight abdominal segment (A8) of the animal. The anterior portion of the dorsal vessel, known as the aorta, is surrounded by a ring gland organ, which has endocrine function, and a hematopoietic lymph gland. At its most anterior point, the dorsal vessel ends in an outflow tract, through which haemolymph can exit and circulate throughout the body. Posteriorly, the heart

lumen is broader, and comprises the heart proper. Abdominal segments 5-8 contain inflow tracts or "ostia" through which haemolymph enters the heart. Seven pairs of filamentous muscle fibers called alary muscles attach the heart to the dorsal epidermis of the animal, thereby stabilizing its position within the body cavity (Tao and Schulz, 2007).

Precursor heart cells first appear during stage 12 of embryonic development, (following gastrulation), at the lateral part of the mesoderm, or "cardiogenic region". At stage 13, the precursors of cardioblast cells become polarized and elongated, developing small leading processes which extend dorsally. This results in a uniform migration of bilateral rows of cardioblasts toward the dorsal midline. Distinguishable from surrounding myoblasts, pericardial cells remain round and unpolarized, but also migrate toward the midline, following behind their contractile cardioblast partners. During these early developmental stages, a transient extraembryonic tissue known as the amnioserosa covers the dorsal surface of the embryo. At stage 14, cells of the amnioserosa begin to die, taking on a columnar appearance and invaginating ventrally. During this time, cardioblasts and pericardial cells proceed to migrate toward the midline to join their contralateral partners, and slide between the invaginating amnioserosa cells which are located ventrally, and the epidermis, which covers the dorsal aspect of the embryo. At stage 15, contralateral pairs of cardioblast cells meet at the dorsal midline via their dorsal leading edges. Trailing edges of cardioblasts curve ventrally at stage 16, coinciding with the formation of adherens junctions and a lumen, which enlarges during later stages of development (Rugendorff et al. 1994; Haag et al. 1999). Dorsal vessel formation is

complete by stage 17, when the lumen is distinctly enclosed by cardioblasts, and the organ initiates synchronized contractions (Rugendorff et al., 1994).

Role of Slit and Robo in the heart

Development of the dorsal vessel is guided by a program of coordinated cell adhesion and migration – processes which are controlled by intercellular signaling and regulated gene expression. Previous research on the genetic control of *Drosophila* heart development has offered insights into how gene inactivation can perturb dorsal vessel morphogenesis (Zaffran and Frash, 2002; Bodmer et al., 2005; Santiago-Martinez et al., 2006; MacMullin and Jacobs, 2006). Two important genes known to be associated with cardiac morphogenesis, and expressed in cardioblasts, are *slit* and *robo*. Slit is an extracellular matrix protein, and a ligand for the Roundabout (Robo) family of transmembrane receptors (Rothberg et al., 1990; Brose et al., 1999; Kidd et al., 1999). It was first characterized as a guidance cue and a midline axon repellant in the nervous system (Kidd et al., 1999; Battye et al., 1999). Slit functions as a repulsive ligand for Robo receptors in the central nervous system, and acts both repulsively and attractively in trachea and somatic muscles (Brose et al., 1999; Kidd et al., 1999; Simpson et al., 2000). Two types of Robo receptors are expressed in the *Drosophila* heart: Robo, and Robo2.

Slit and Robo are expressed in cardioblast cells, while Robo2 is localized exclusively to the pericardial cells (Bodmer et al., 2005; Santiago-Martinez et al., 2006). During cell migration and before contralateral cardioblasts meet at the dorsal midline, Slit and Robo are expressed uniformly throughout the cytoplasm of cardioblasts, and at the contact site

between cardioblasts and pericardial cells. Robo is also expressed in pericardial cells. However, as the bilateral rows of cardiac cells meet at the dorsal midline at stage 16, Slit becomes localized to the midline. In a similar pattern of expression, Robo strongly enriches the apical (dorsal) surface of cardioblasts, although it can still be detected on pericardial cell surfaces (Bodmer et al. 2005; Santiago-Martinez et al., 2006). Unlike Robo and Slit, Robo2 remains localized to the pericardial cells both before and after the alignment of contralateral pairs at the dorsal midline. Interestingly, when *robo2* (also known as *lea*), is ectopically expressed in cardioblasts, cardioblast rows are driven laterally away from the midline to a distance normally maintained by pericardial cells. In contrast, in mutants for *robo2*, pericardial cells were seen to move toward the midline further than expected. These results suggest that the role of *robo2* may be to maintain the position of pericardial cells behind cardioblasts (Santiago-Martinez et al., 2006).

Several studies have shown that the Slit-Robo signaling pathway is essential during cardiac morphogenesis, specifically for normal cardioblast migration, alignment, adhesion, and lumen formation. (Bodmer et al., 2005; MacMullin and Jacobs, 2006; Santiago-Martinez et al., 2006). Both homozygous *slit* mutants, as well as mutants doubly heterozygous for *robo,lea* exhibited phenotypes with highly irregular cell arrangements, as compared to wild type animals. Observable abnormalities included gaps or breaks within the normally highly organized and continuous bilateral rows of cardioblasts, inappropriate migration of cells into (or across) the midline, clumping of cells, and other lesions indicative of disrupted heart development (Bodmer et al., 2005; MacMullin and

Jacobs 2006). Abnormal localization of several cell polarity markers has also been reported (Bodmer et al., 2005; Medioni et al., 2008).

The Slit protein consists of four distinct domains: four leucine-rich repeat (LRR) regions at the N-terminus, followed by seven epidermal growth factor (EGF)-like repeats, a laminin-like globular (G) domain, and a C-terminal cystine knot (Rothberg et al. 1990 ; Hohonester et al. 2006). In the central nervous system, Robo is known to bind to the second leucine-rich repeat of Slit (Hohonester et al. 2006), thus *slit* transgenes lacking the LRR domain cannot bind Robo, and thus are unable to restore normal Slit function (Battye et al., 2001). In the heart, Slit localization is disrupted from its expected wild type pattern in *robo, lea* mutants. In accordance with this, *slit* mutants also exhibit inappropriate Robo localization (Bodmer et al., 2005). However, in one study, a significant rescue phenotype was observed when a *slit* transgene containing internal deletions of the LRR was expressed in homozygous *slit* mutants (MacMullin and Jacobs 2006), indicating that Slit may function independently of Robo in this organ. In addition, *slit* was not shown to interact strongly with genes required for Robo signaling, as mutants heterozygous for null alleles of *slit* and *lea,* or *slit* and downstream second messengers of *lea* (Disabled, Ras, and Dock), appeared to compromise heart development to a very small extent, or not at all (MacMullin and Jacobs 2006).

Slit-Robo signaling has been shown to be important for proper lumen formation during dorsal vessel morphogenesis. Specifically, it has been shown that Slit and Robo repel contralateral cardioblasts from each other in their central apical domain region, by inhibiting E-cadherin mediated adhesion in this region, and consequently allowing for the

formation of a lumen (Santiago-Martinez et al., 2008). Another recent study proposed a similar model for cardiac tube formation in which Slit-Robo signaling inhibits E-Cadherin mediated adhesion, but in addition the authors suggest that a parallel Slit-Robo pathway participates in regulation of the actin cytoskeleton and triggers cardioblast cell shape remodeling which is necessary for lumen formation (Medioni et al., 2008).

1.3 Interaction of Slit, Robo, and Syndecan

Recently, a co-receptor for Slit has been identified as the heparan sulphate proteoglycan (HSPG), Syndecan (Steigemann et al., 2004, Johnson et al., 2004; Rhiner et al., 2005). Convincing evidence from genetic studies suggests that HSPGs play an important role in Slit-Robo signaling. In experiments with *C. elegans*, zebrafish, and mice, ablation of enzymes involved in HS biosynthesis resulted in defects similar to those produced in animals deficient for Slit and Robo (Bulow et al., 2002; Inatani et al., 2003; Bulow and Hobert 2004; Lee et al., 2004). Moreover, expression for Robo and Syndecan overlaps in the *Drosophila* nervous system (Steigemann et al. 2004; Johnson et al. 2004). To further substantiate this observation, normal Slit-Robo signaling was shown to require the presence of Syndecan on axons expressing Robo (Steigemann et al. 2004 and Johnson et al. 2004; Rhiner et al., 2005). Molecular studies have shown that both Slit and Robo immunoprecipitate with Syndecan (Johnson et al., 2004). Syndecans function as dimeric, transmembrane cell surface proteins and have two HS chains (Couchman 2003). Experiments have demonstrated a specific, high affinity interaction between the C-terminal domain of Slit and one of Syndecan's HS chains, as well as a weaker interaction

between the other HS chain and the LRR domain of N-terminal Slit (Hussain et al. 2006). Although this interaction is weaker, it is potentially more specific, as experiments involving proteolytic cleavage of Slit have shown that it is the N-terminal and not C-terminal fragment that remains bound to cell surfaces, despite its weaker affinity to HS (Brose et al., 1999). Based on this current knowledge of the interaction between Slit and Syndecan, it has been hypothesized that HS binding may play a dual role in Slit-Robo signaling: while the C-terminal, high affinity HS binding site may serve to concentrate Slit at the cell surface, the weaker but perhaps more specific HS-LRR site may be required for the formation and stability of a ternary Slit-Robo-HS signaling complex.

1.4 Slit and Syndecan have integrin-based adhesive functions

Integrins are transmembrane glycoproteins that exist as αβ heterodimers (Morgan et al., 2007). The extracellular domain of integrins interacts with extracellular matrix (ECM) glycoproteins and cell-surface proteins (Humphries et al., 2006), while the cytoplasmic domain interacts with components of the actin cytoskeleton (Morgan et al., 2007). These bilateral linkages allow the integrins to carry out two primary functions, which are to attach cells to the ECM, and to transduce signals from the ECM to the cell (Mitra et al., 2005). When the extracellular domain of integrins binds to the ECM, conformational changes occur in the cytoplasmic domains, altering their interaction with cytoskeletal or other proteins that regulate cell adhesion, growth and migration. At the same time, signals generated inside the cell can alter the activation state of some integrins, affecting their affinity for their extracellular ligands. Thus, integrins are able to

signal across the membrane in both directions, "inside-out" and "outside-in" (Morgan et al., 2007).

Previous experiments have shown that a strong mutant phenotype is produced in flies doubly heterozygous for *slit* and the integrin genes *scab* (αPS3) and *myospheroid* (βPS1), or *slit* and integrin ligands, including Laminin and Collagen. Similar mutant phenotypes were observed in *Drosophila* heterozygous for *slit* and intracellular messengers such as Talin and ILK. These findings suggest that *slit* may be involved in integrin-based adhesion and plays a role in linking the cell to the ECM (MacMullin and Jacobs 2006).

Recent studies have shown that syndecans participate in cooperative signaling with integrins in order to elicit cellular responses to the ECM. In support of this, there is evidence that cell adhesion requires the presence of both types of receptor. In fact, many ECM molecules have been found to contain binding sites for both syndecans and integrins (Morgan et al., 2007). A clear synergy has been demonstrated between the signaling cascades of the two receptors *in vitro* (Morgan et al., 2007). Interestingly, there have even been reports that the proteins which make up the extracellular domains of syndecans act as ligands for integrins (Beauvais et al., 2004; McQuade et al., 2006; Whiteford and Couchman, 2006).

1.5 Thesis objectives

The primary objective of this thesis was to gain a better understanding of the coordinated sequence of events which lead to development of the dorsal vessel. Specifically, we sought

to gain further insight into the mechanisms underlying abnormalities in cell migration, alignment, and adhesion in *slit*, *robo,lea* and *syndecan* mutants. We used time lapse confocal microscopy to observe cardial cell shape, morphology, migration, and behavior with respect to neighbouring or surrounding cells in mutants and wild type animals. Of particular interest to us with respect to cell shape and morphology, was the appearance and behavior of the leading edges of cardioblast cells. Studying the orientation, size, and behavior of the filopodia of these cells during migration, and during contact with contralateral partners in wild type and *slit* mutant animals, was the second aim of this study.

Finally, we aimed to further understand the role of Syndecan, a recently discovered co-receptor for Slit, in the Slit-Robo pathway. We first examined time lapse movies of homozygous *syndecan* mutants to see how dorsal vessel defects compared to those seen in homozygous *slit* mutants and mutants doubly heterozygous for *robo,lea*. We then set out to elucidate the nature of the genetic interaction between *robo, lea*, and *syndecan.* As mentioned earlier in this chapter, it has been hypothesized that Slit and Robo may form a signaling complex which is stabilized by Syndecan (Hohenester et al., 2006). Syndecan and Slit have also been shown to have integrin-based functions (MacMullin and Jacobs, 2006; Morgan et al., 2007), and to work independently of Robo (MacMullin and Jacobs, 2006, Komosa, 2008). In order to gain an understanding of the genetic interaction between the receptors of Slit, we compared the developmental phenotypes of mutants triply heterozygous for *syndecan, robo,* and *lea* to those homozygous for *syndecan* and doubly heterozygous for *robo,lea*. Elucidating the functional role of Syndecan in relation

to Slit and Robo is of importance, since Slit and Robo have been shown to be required for many aspects of dorsal vessel development (Bodmer et al., 2005; MacMullin and Jacobs, 2006; Santiago-Martinez et al., 2008; Medioni et al., 2008). It is possible that Syndecan has a role in one or all of the same essential processes.

Chapter 2

Materials and Methods

2.1 *Drosophila melanogaster* strains

Several *Drosophila* strains were created for the purpose of studying heart development through the use of time-lapse confocal microscopy (refer to appendix 2 for genetic schemes). The lines created were: sli^2/CyO_{GFP}; *tupGFP/TM3*, sdc^{97}/CyO_{GFP}; *tupGFP/TM3,* and *robo,lea/*CyO_{GFP}; *tupGFP/TM3. tupGFP* is a nuclear GFP marker under the control of the dorsal vessel transcriptional enhancer of the *tailup (tup)* gene (Tao and Schulz, 2007). This marker is expressed in all cell types of the heart: cardioblasts, pericardial cells, lymph glands, and alary muscles. The crossing of adult flies in each of the lines constructed produced embryos mutant for both copies of the particular gene of interest, in a *tupGFP* background. This allowed for the study of the behavior, morphology, and migration patterns of cardioblast and pericardial cell nuclei in mutant embryos. Another strain made was sli^2*/CyO; Dmef2GAL4/TM3* (App. 2). *Dmef2* is a muscle specific transcription factor expressed in all myocardial and other muscle cells (Bour et al., 1995; Lilly et al., 1995). Fusion of *Dmef2* to a *GAL4* construct produced a cardiac cell driver which was used to promote the expression of a membrane targeted GFP (*UAS CD8 GFP*). This was achieved by crossing the sli^2*/CyO; Dmef2GAL4/TM3* strain to flies of a recombinant strain previously constructed by Allison MacMullin, (sli^2, *UAS CD8 GFP/CyO*) (Appendix 2). The primary objective of studying heart development in the progeny of this particular cross was to observe the morphology and behavior of

cardioblast leading edges. Particular interest was in the orientation, size, and behaviour of the filopodia of these cells during migration.

2.2 Embryo collection and mounting procedures

Prior to collection of embryos for time lapse observations, mounting slides were constructed in the following manner. A thin strip of Gridstick adhesive (Pelco) was applied across the center of an 18 x 22 cm coverslip using the tip of a paintbrush. Round, plastic wells which were made by trimming the open ends of 1000 µL pipette tips, were then fixed onto each coverslip surrounding the stick adhesive, by applying Permount mounting medium to the outer rim.

Adult flies from the strains of interest were placed into 100 ml plastic beakers that were capped by petri dishes filled with apple juice agar (2.25% w/v agar, 2.5% w/v sucrose, 25% v/v apple juice), and a small smear of yeast paste. Adults were allowed to lay eggs on the agar medium, and plates were changed 1-2 times daily in order to obtain embryos representative of various developmental stages. Once embryos were available, they were collected from the agar plates with a paintbrush and smeared across double-sided tape attached to a glass slide. A Nikon dissecting microscope with a GFP filter was used to visualize and identify embryos of interest. For mutant strains, embryos marked by actin GFP balancers were used to exclude heterozygous individuals. Embryos were then dechorionated and mounted with their dorsal surfaces facing down onto the strip of adhesive that was applied to the mounting slide, allowing them to stay firmly attached to the coverslip surface. The surrounding plastic wells were then filled with oxygenated

halocarbon oil which prevented the embryos from drying out, and kept the embryos alive for the duration of the time lapse experiments.

2.3 Time lapse confocal imaging

All time lapse studies were carried out using the Leica DMI 6000 B spinning disc confocal microcope, equipped with a Hamamatsu C9100-12, back-thinned EMCCD camera. GFP in embryos was visualized using the Semrock 536/40 emission filter. We used a 40 x 0.6 NA Ph Fluotar lens for all movies except those made for examining cellular protrusions (leading processes), where we used a higher magnification (63 x 1.3 NA DIC glyc HCX Pl-Apo) lens. Images were acquired using Volocity4 Improvision software. Due to the thickness and density of embryo samples, we acquired images using a z-series, scanning a number of slices 1.5 μm thick with a frequency of either 30 seconds or 1 minute. Movies were saved in .avi format and analyzed and reformatted using ImageJ.

2.4 Measurement of cell migration speed

ImageJ software was used for all quantitative analysis of time lapse images. Migration speed of cardioblast cells was measured by drawing a straight line from a particular cell's position at time t=0 to its position exactly 60 minutes later. Measurements were obtained in pixels, and were then converted to micrometers by multiplying by 0.387585, (the pixel size for the 40x lens utilized to capture images). In order to maintain consistency, measurements of cell migration were taken within

segments A2-A5 of all embryos. The distance traveled by six randomly selected cells from each embryo was measured within these segments. A different embryo was used for measurements of migration speed at each stage of development (13-14, 14-15, 15-16, 16-17), except in *robo,lea* mutants, where data was only available for stages 15-16 and 16-17. Statistical significance of differences in migration speed between wild type and mutants was determined by applying the Mann-Whitney test for non-parametric samples, using Minitab® statistical software.

2.5 Phenotypic scoring of dorsal vessel defects

Dorsal vessel phenotypes were scored based on a technique adapted from MacMullin and Jacobs (2006). Mutants in this study exhibited a variety of defects related to heart assembly, including gaps, cell clumping, cells in the midline, lumen blisters, flattening of nuclei, absence of a GFP intensity pattern, lateral curvature of the dorsal vessel, and multiple lumens. Six embryos were scored for the presence or absence of these defects in each genotypic class. The presence of a particular type of defect received a score of 1, while the absence of that defect was given a score of 0. The severity of the phenotype for each genotype was then determined by summing the total of all scores, and dividing by 40, to obtain a number between 0 and 4. The closer the ranking to 4, the more severe the phenotype. Penetrance was a value obtained by calculating the fraction of embryos in each genotypic class that had two or more different types of defects.

Chapter 3

Results

3.1 Time lapse observations of wild type heart development

In order to understand the sequence of events that lead to the formation of a normal, fully functioning dorsal vessel, we reviewed a total of approximately 6.5 hours of film by looking at time lapse movies of wild type heart development in 6 different embryos. In these movies, wild type embryos expressing *tupGFP (+/+; tupGFP),* were studied at various developmental stages. Only cell nuclei of heart forming cells were visualized with this strain. The following observations were made:

Stage 13 – A continuous row of cardioblast cell nuclei becomes visible at both the right and left most lateral areas of the dorsal surface, with each row situated approximately 70 μm from the dorsal midline. Pericardial cell nuclei, which flank cardioblasts laterally, also become visible, but appear flatter than the nuclei of cardioblasts (Figure 1 A; Movie 1). As development progresses, both cardioblast and pericardial cell nuclei migrate toward the midline as a continuous sheet. At the same time as cell rows travel toward their contralateral partners, each individual cardioblast nucleus can be seen oscillating back and forth repeatedly at a frequency of about once every minute, with nuclei momentarily moving at most half a nuclei length in front of the cardioblast row, then returning immediately to their original positions.

Stage 14 – Bilateral cell rows continue to migrate toward each other and the dorsal midline. Cells which will make up the eventual ring gland appear in the anterior heart

region and begin to organize themselves into a clumped, mound-shaped structure. Pericardial cell nuclei take on a more rounded appearance (Figure 1 B; Movie 1). A unique pattern in GFP intensity is observable in the mid-abdominal segments of the heart (A2-A5), where a pair of nuclei with a high GFP intensity are followed by four nuclei of obviously lower intensity. This pattern is repeated four times throughout segments A2-A5 (Figure 2 A; Movie 1). Interestingly, this difference in GFP intensity corresponds to a distinction in the genetic identity of these cells. While the pair of brighter nuclei express Seven-up *(svp),* an orphan steroid hormone receptor, the following four less intensely glowing nuclei express the homeodomain protein Tinman *(tin)* (Gajewski et al. 2000; Tao and Schulz, 2007). No difference in GFP intensity is seen in the anterior-most (T2-A1) or posterior-most (A6-A8) segments, where all nuclei appear to express the same level of GFP.

Stage 15 – Alary muscles, which serve to anchor the dorsal vessel in the body cavity, begin to form during this stage. The cells making up these muscles can be seen moving perpendicularly to the dorsal vessel, in the body wall (Figure 1. C, arrows). Alary muscles appear to be formed by cells migrating in opposite directions along the body wall. Cells which appear to originate from the area near the pericardial cells migrate laterally while cells coming from the opposite direction move medially toward them. Cells moving in both directions flatten while migrating and take on a rounded appearance once in contact (Figure 1. C, arrows; Movie 2).

Stage 16-17 – Alary muscles continue to form. Bilateral rows of cardioblasts (and the pericardial cells flanking them), continue to migrate dorsally until they meet at the dorsal

midline. The overall intensity of GFP increases in all cells of the dorsal vessel, making it more difficult to distinguish between *svp* and *tin*-expressing cells (Figure 1. D,E ; Movie 3). A drawing of a mature dorsal vessel at stage 17 can be seen in Figure 1. F.

The events of heart development described above require approximately 3.5-4 hours to reach completion, with each developmental stage proceeding in or under 60 minutes (Figure 3).

Figure 1. Stages of wild type dorsal vessel development.

Stages of wild type dorsal vessel development showing the nuclei of cardioblasts and pericardial cells (expressing *tupGFP*). (A) Stage 13, (B) Stage 14, (C) Stage 15, arrows indicate forming alary muscles, (D) Stage 16, (E) Stage 17. Anterior is to the upper left, posterior is to the lower right in A-C. In D,E anterior is up, posterior is down. Scale bar for panels A-E: 2.6 pixels = 10 micrometers. (F) Drawing (adapted from Tao and Schulz, 2007) showing the structure of the mature dorsal vessel, including the position of cardioblasts and pericardial cells, lymph gland cells, and ring gland cells. 'a' indicates the portion of the dorsal vessel referred to as the aorta, 'h' refers to heart proper. Anterior is to the left.

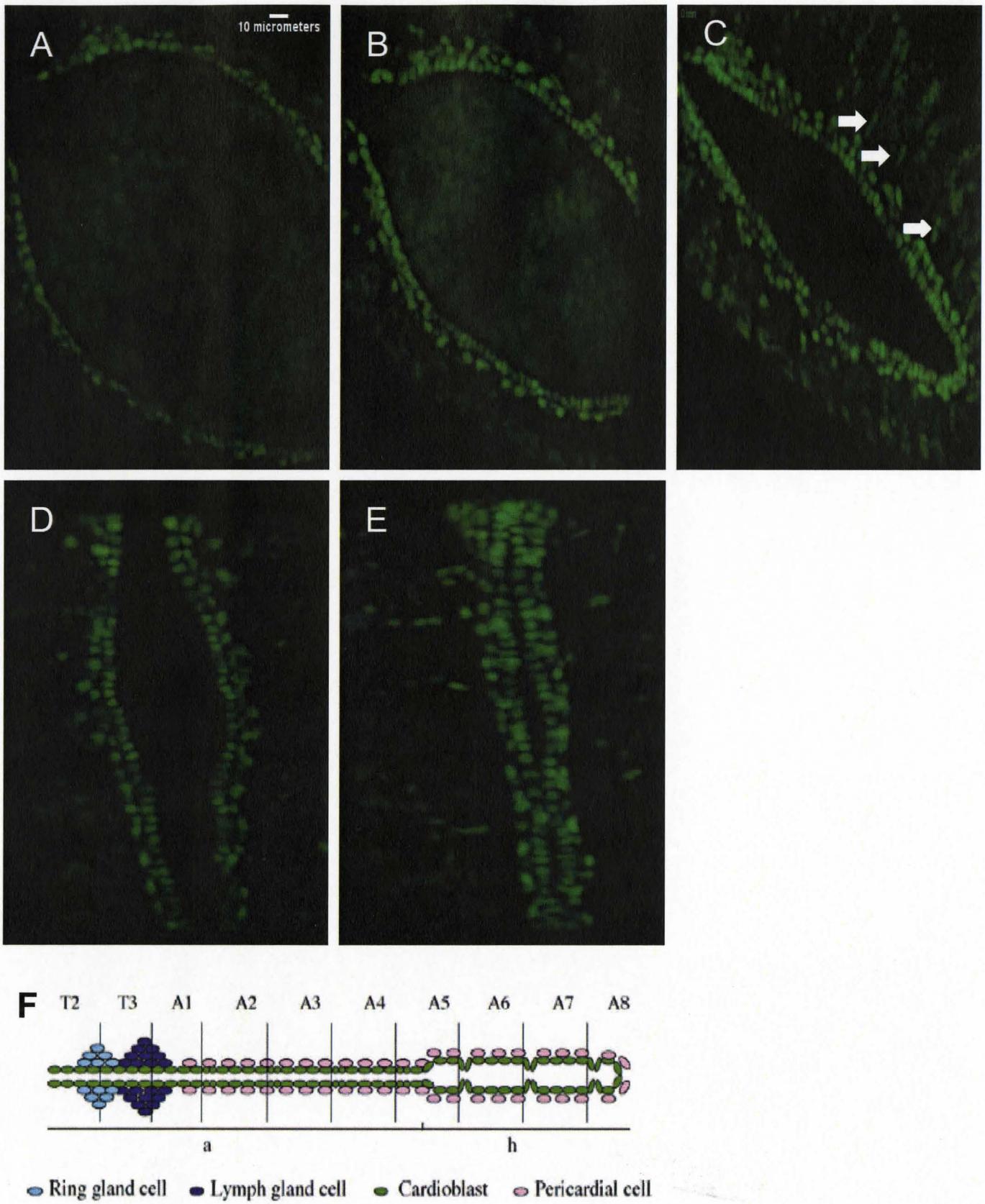
A
10 micrometers
B
C
D
E
F
T2
T3
A1
A2
A3
A4
A5
A6
A7
A8
a
h
Ring gland cell
Lymph gland cell
Cardioblast
Pericardial cell

Figure 2. GFP intensity difference of cardioblasts in segments A2-A5.

In wild type animals (A), a unique pattern in GFP intensity can be observed in the mid-abdominal segments of the dorsal vessel (A2-A5). A pair of nuclei with a high GFP intensity (putative *svp*-expressing cells, denoted by arrows), are followed by four nuclei of obviously lower intensity (putative *tin*-expressing cells). This pattern in GFP intensity is repeated four times throughout segments A2-A5. In *slit* (B), and other mutants, this pattern in GFP intensity is absent. Both embryos shown are at stage 14. Anterior is to the upper left, posterior is to the bottom right. Scale bar for A,B: 2.6 pixels = 10 micrometers.

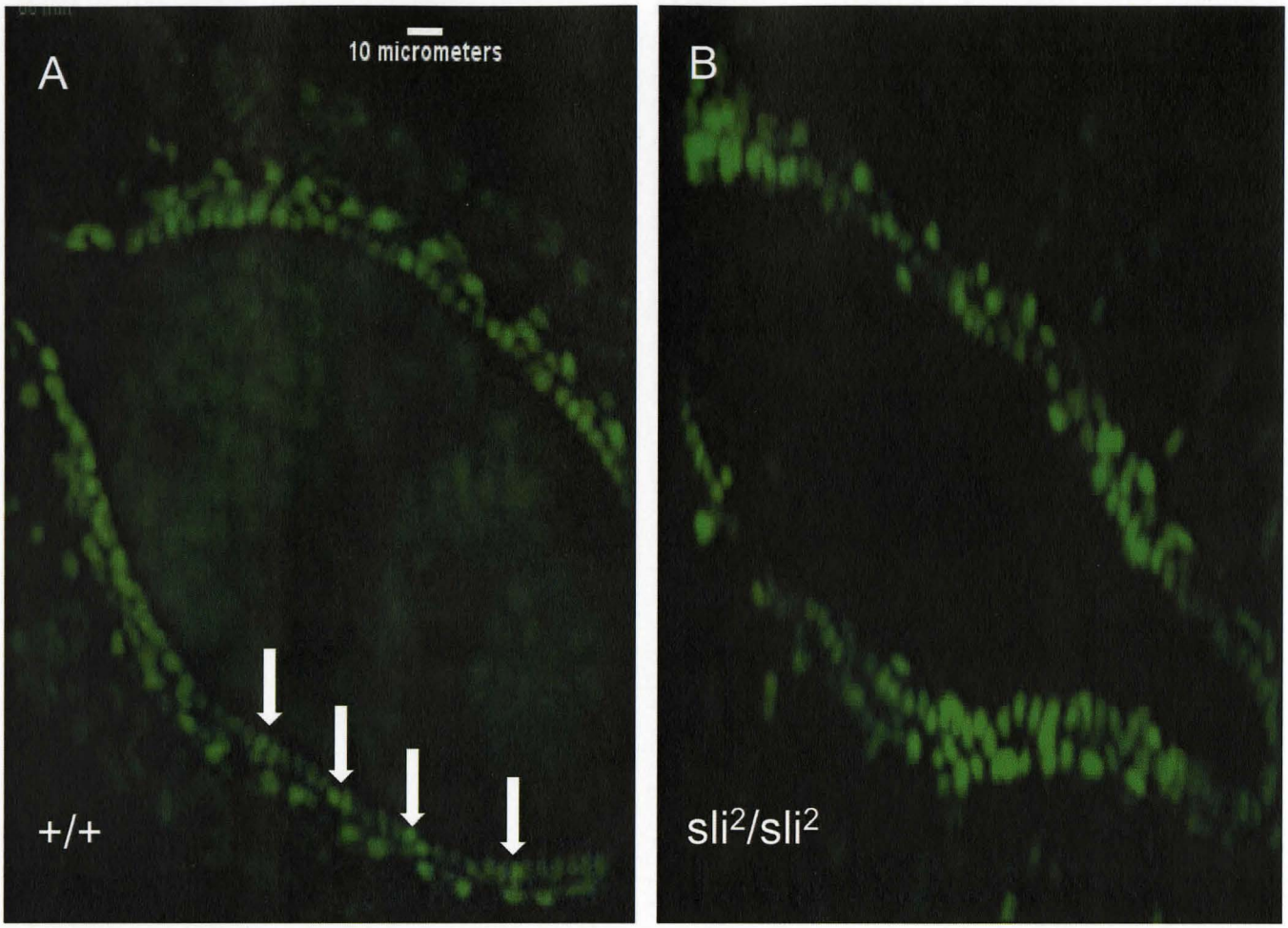
A
10 micrometers
+/+
B
sli2/sli2

Figure 3. Time course of dorsal vessel development

This graph shows the time taken to complete each of the developmental stages indicated (in minutes) for wild type and mutant animals. Whenever possible, a different representative embryo was used to measure the time for each developmental stage in each genotypic class. However in some cases, data was only available for some stages, and not others.

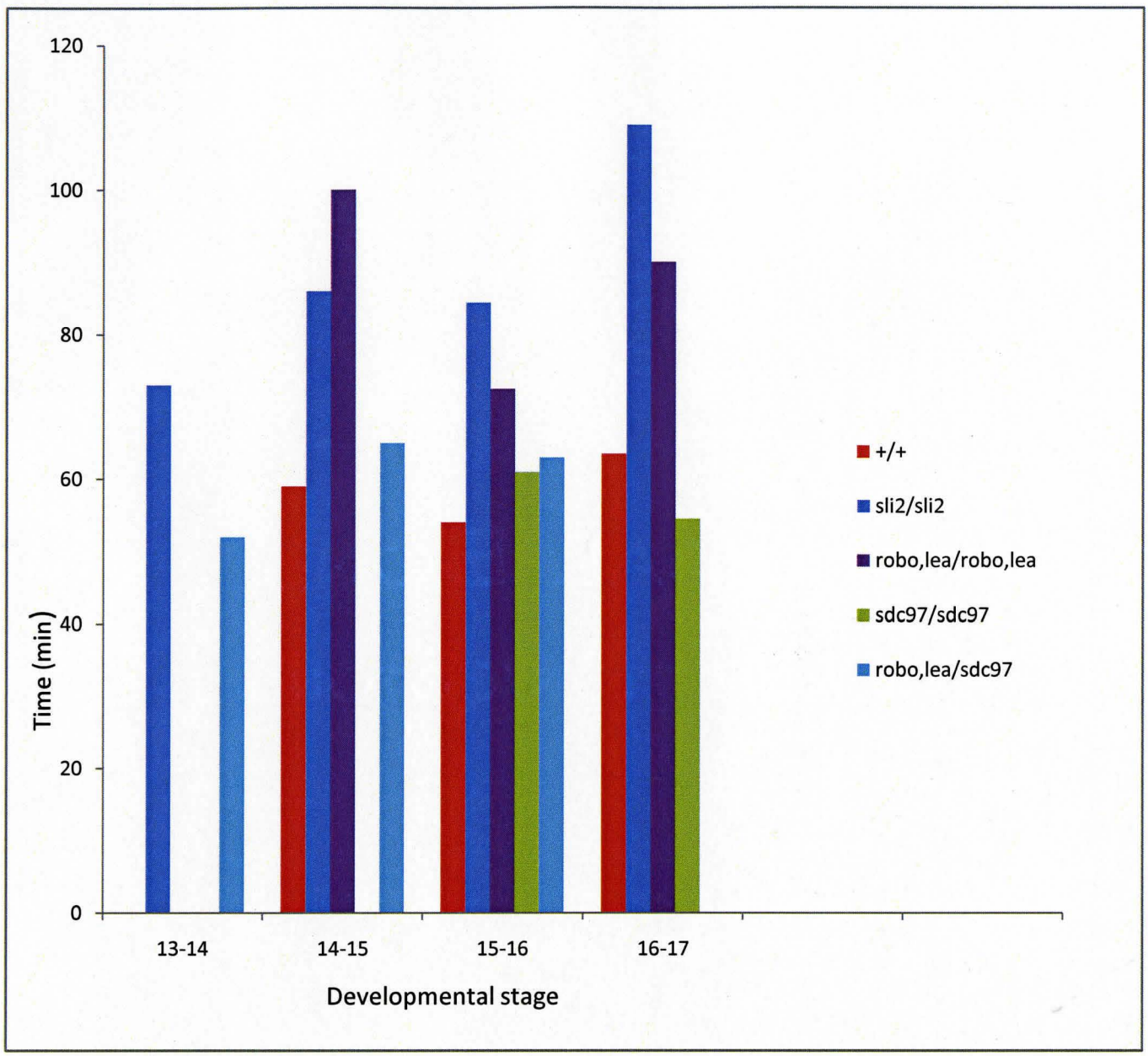
120
100
80
60
40
20
0
Time (min)
13-14
14-15
15-16
16-17
Developmental stage
+/+
sli2/sli2
robo,lea/robo,lea
sdc97/sdc97
robo,lea/sdc97

3.2 Heart development in *slit* mutants

In order to gain further insight into the functional role of Slit during heart morphogenesis, we examined time lapse movies of dorsal vessel development in embryos mutant for both copies of the *slit* gene. As in wildtype, visualization of the dorsal vessel was made possible because embryos expressed the nuclear GFP marker, *tupGFP*. Dorsal vessel formation in *slit* (sli^2/sli^2;*tupGFP/TM3*) mutants resulted in observable abnormalities in cardioblast alignment, migration, and adhesion. Commonly observed defects included clumping of cardioblasts, gaps in the normally continuous cardioblast rows, cells migrating across the midline to the contralateral cell row (or simply remaining in the midline between cell rows) (Figure. 4 ; Table 1; Movie. 4), absence of the GFP intensity difference between *svp* and *tin*-expressing cells (compare Figure 2 B with Figure 2 A), lateral curvature or twisting of the dorsal vessel, lumen blisters (failure of the lumen to close), formation of multiple, separate lumens (Figure 4; Table 1; Movie. 4), and flattened nuclei (Figure 5). Flattened nuclei were observed in lone cells that had migrated out of the cardioblast row (Figure 5 B). This nuclear morphology likely mimicks the shape of the actual cell membrane, which can also be seen to flatten and elongate in lone cells of *slit* mutants expressing membrane-targeted *UAS CD8 GFP* (compare Figure 6 B with Figure 6 A). This behavior may be associated with a cell's attempt to find neighbouring cells to adhere to or align with, since the nucleus reverts to a normal, rounded appearance once a lone cell has contacted a partner (Figure 5 C).

Dorsal vessel development in *slit* mutants was delayed at each stage, in comparison to wild type (Figure 3). While development from stage 15 to 16 proceeded in

approximately 60 minutes in wild type (Figure 3; Movie 2), the same stage proceeded for over 100 minutes in *slit* mutants (Figure 3; Movie 6). This observable developmental delay corresponded to a slower speed of cardioblast cell migration at all stages of *slit* development, compared to wild type (Figure 10). For example, during stage 16-17, *slit* mutant cardioblasts traveled at migration speeds ranging between 3.65-8.18 μm/hr, while wild type migration speed at this stage ranged between 8.22-15.27 μm/hr (Figure 10). We determined the differences in migration speed between wild type animals and *slit* mutants to be statistically significant at all stages of development ($p<0.05$), by using the Mann-Whitney test (Appendix 3).

Figure 4. Dorsal vessel defects in *slit* mutants

Defects typically observed in *slit* (sli^2/sli^2;*tupGFP/TM3)* mutants included cell clumping (asterisk), gaps in cardioblast rows (~), cells migrating across the midline or remaining in the midline between contralateral rows (x), flattening of nuclei (arrow), and lumen blisters, or failure of the lumen to close (diamond). All embryos shown are stage 16-17. Anterior is to the upper right, posterior is to the lower left. Scale bar for A-D: 2.6 pixels = 10 micrometers.

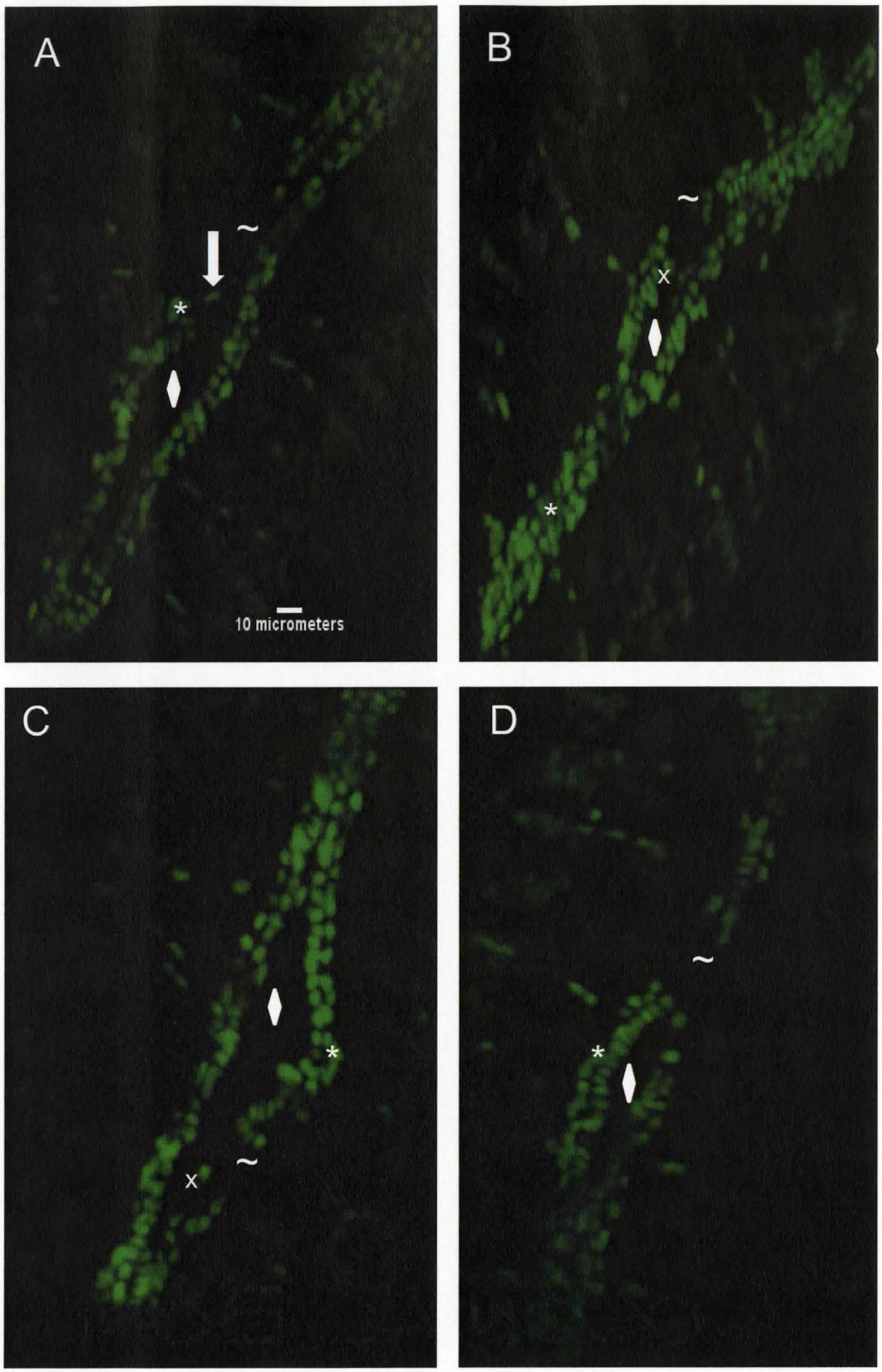
A
B
C
D
10 micrometers

Table 1. Frequency of heart defects in mutants

This table shows the frequency of dorsal vessel assembly defects commonly observed in *slit, robo,lea, syndecan,* and *robo,lea/syndecan* mutants, as well as the severity[a] and penetrance[b] for each genotype.

[a] Severity: Measure of the level of abnormal dorsal vessel formation for each genotype. Embryos were ranked on a scale of 0 to 4, with higher rankings representing a higher number of defects per embryo. 6 embryos were scored for each genotype.

[b] Penetrance: The fraction of embryos that had two or more observable dorsal vessel defects.

Genotype	+ / +	*sli*^{2}/*sli*^{2}	*robo,lea/robo,lea*	*sdc*^{97}/*sdc*^{97}	*robo,lea/sdc*^{97}
Severity[a]	0.15	1.50	2.05	1.55	0.9
Penetrance[b]	0.16	1.00	1.00	1.00	1.00
Gaps	0	6	12	5	6
Nuclei flattening	2	14	20	15	12
Cell clumping	3	10	14	11	9
Midline crossings	1	13	18	16	0
Curved lumen	0	3	3	2	0
Multiple lumens	0	5	6	4	0
Lumen blister	0	4	3	4	3
Unexpected GFP pattern	0	5	6	5	6
Number of embryos	6	6	6	6	6

Figure 5. Flattened nuclei phenotype of lone cardioblasts

Lone cardioblasts that had migrated out of their cardioblast row had nuclei which were observed to take on a flattened appearance. Once lone cells encountered a cardioblast partner, the nuclei reverted back to a rounded shape. This behavior is presumably associated with the cell assuming a migratory phenotype while searching its surroundings for cardioblast partners. (A) shows two lone nuclei, at t=0 min. (B) is a magnified picture of the area boxed in (A). Arrows indicate lone cells. (C) shows the flattened nuclei of the lone cells (arrows) at t=84 min, before they had made contact with other cells. (D) The lone cells' nuclei revert back to a rounded appearance (arrows) once they have made contact with other cardioblasts. The dorsal vessel shown is from a stage 16 *slit* mutant, although the same nuclear behaviours were also observed in *robo,lea* and *syndecan* homozygotes, and *robo,lea/syndecan* triple heterozygous mutants. Anterior is to the upper left, posterior is to the lower right. Scale bar: 2.6 pixels = 10 micrometers.

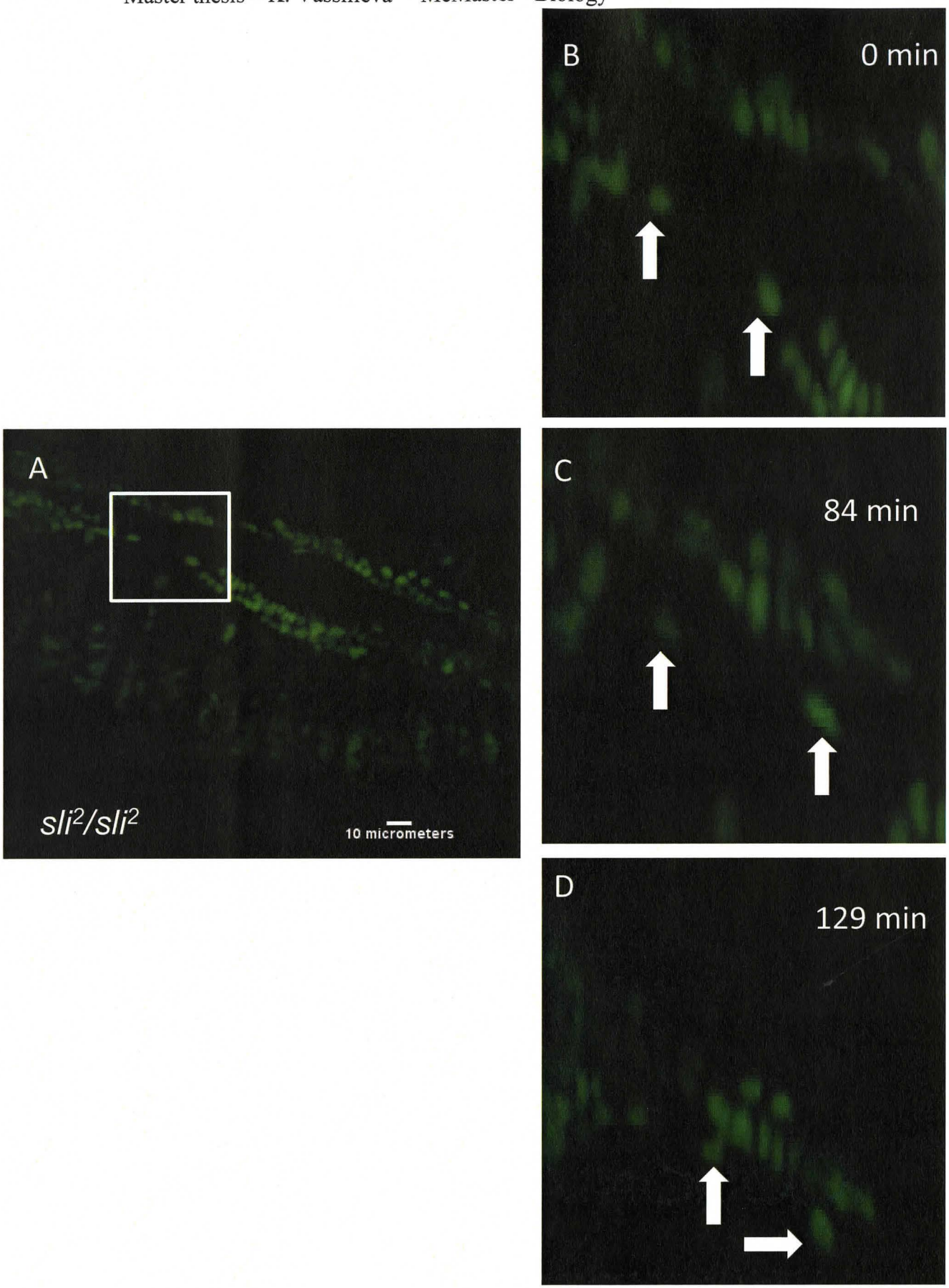
A
sli²/sli²
10 micrometers
B
0 min
C
84 min
D
129 min

Figure 6. Elongated morphology of cardioblasts expressing membrane-targeted *UAS CD8 GFP*.

While cardioblasts of wild type embryos retained a round morphology (A), *slit* mutant cardioblasts exhibited an elongated morphology in lone cells which had left the cardioblast row, or cells located around gaps (B). This cellular morphology likely coincides with the flat nuclear morphology seen in mutant embryos expressing *tupGFP*. Both embryos shown are stage 16. Anterior is up, posterior is down. Scalebar for A, B: 5.6 pixels = 10 micrometers.

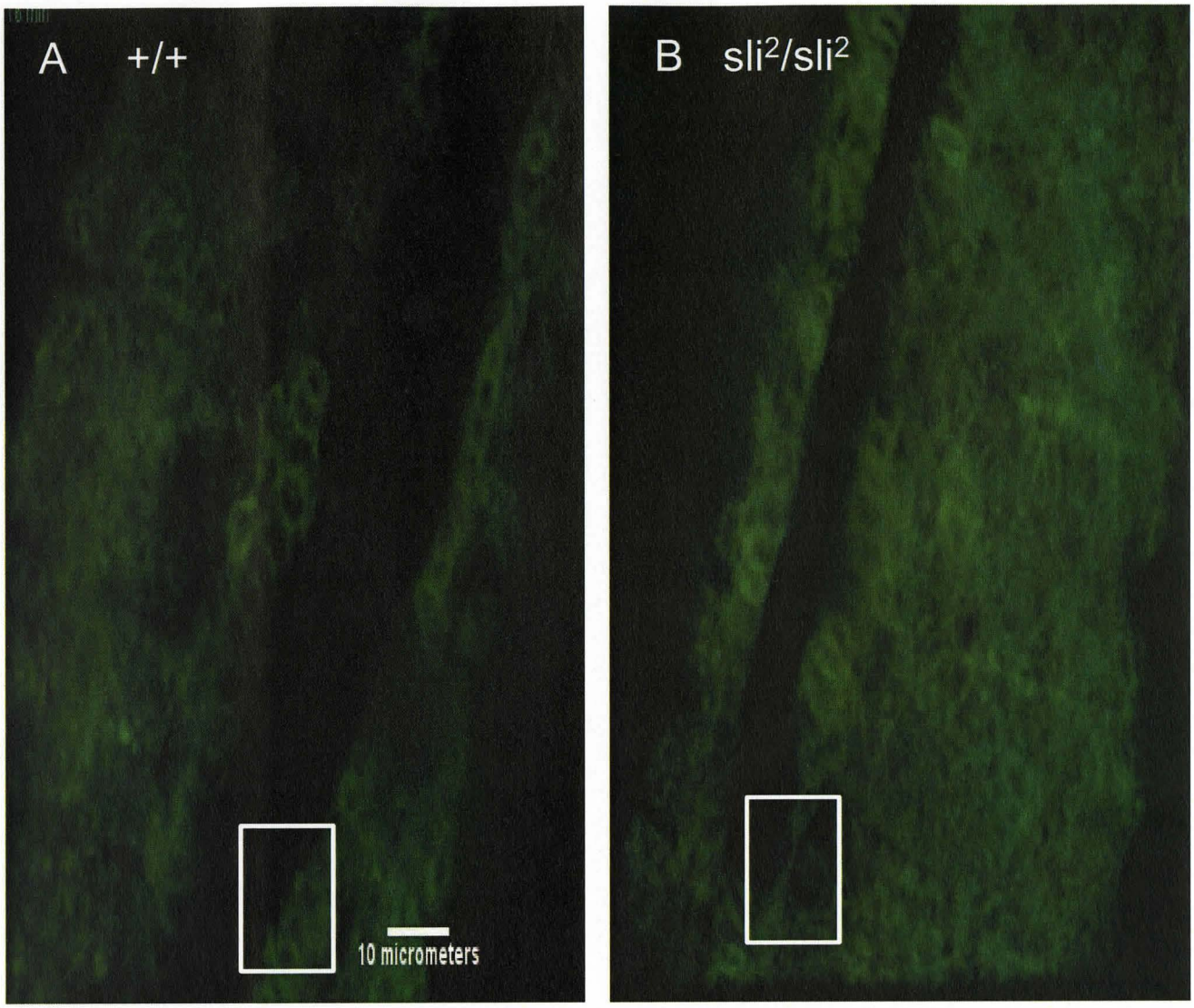
A +/+
10 micrometers
B sli2/sli2

3.3 Heart development in *robo,lea* mutants

In addition to ascertaining the functional role of *slit*, we were interested in the role of the *robo* and *lea* genes during heart morphogenesis. Previous experiments have shown that mutants homozygous for either gene alone present mild phenotypes (Bodmer et al., 2005; MacMullin and Jacobs, 2006). However, it has also been shown that the dorsal vessel defects observed in mutants doubly mutant for both *robo* and *lea* resemble those seen in *slit* homozygous mutants (MacMullin and Jacobs, 2006). In our examination of time lapse movies, we found that the types of dorsal vessel defects in *robo,lea (robo,lea/robo,lea; tupGFP/TM3)* mutants were in fact the same as those seen in *slit* mutants (Figure 7; Movie 7). However, when we scored embryos based on the number of defects we observed, we found that the severity of mutant phenotypes was greater in *robo,lea* mutants (2.05), than *slit* mutants (1.50) (Table 1).

Mutants for *robo,lea* exhibited a slower rate of development for stage 15-16 (slightly over 70 min), than wild type animals (approximately 60 min) (Figure 3; Movie 7). However, *robo,lea* mutants developed faster than *slit* mutants at this stage (Figure 3). The speed of cardioblast migration was not found to differ significantly ($p<0.05$) between *robo,lea* mutants (15.9-22.7 μm/hr, n = 6 cells) and wild type animals (14.6-19.9 μm/hr, n = 6 cells) at stage 15-16, or stage 16-17 (compare 8.60-12.52 μm/hr, n = 6 cells, for *robo,lea* with 8.22-15.27 μm/hr, n = 6 cells, for wild type) (Figure 10).

Figure 7. Dorsal vessel defects in *robo,lea* mutants

Defects in *robo,lea (robo,lea/robo,lea;tupGFP/TM3)* mutants were similar to those observed in *slit* mutants: cell clumping (asterisk) , gaps in rows of cardioblasts (~), cells migrating across the midline or remaining in the midline between contralateral rows (x), flattening of nuclei (arrows), failure of the lumen to close (diamonds), absence of the GFP intensity pattern of *svp* and *tin*-expressing cells (compare A,B,C with Figure 2 A), and inappropriate curvature or shape of the dorsal vessel (compare B with Figure 1 E). All embryos shown are stage 17. Anterior is up, posterior is down. Scale bar: 2.6 pixels = 10 micrometers.

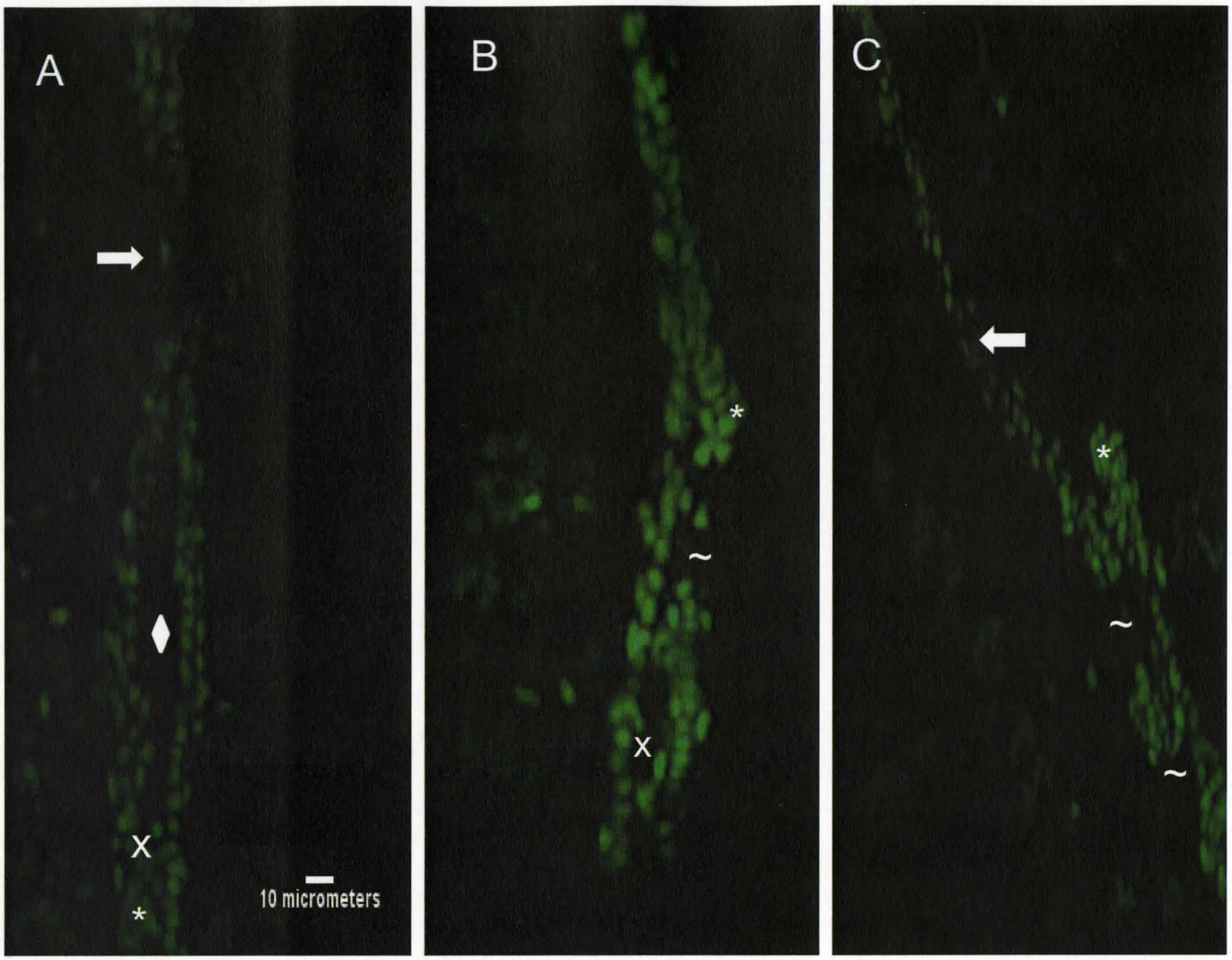
A
B
C
X
*
10 micrometers
~

3.4 Heart development in *syndecan* mutants

The recently discovered HSPG Syndecan has been demonstrated to participate in biochemical interactions with both Slit and Robo *in vitro* (Hohenester et al., 2006). However, the exact nature of the genetic interaction between Syndecan, Slit, and Robo remains largely unknown. Prior to investigating potential genetic interactions between these proteins, we first sought to establish the role of Syndecan during heart morphogenesis. As with *slit* and *robo,lea* analysis, we placed *syndecan* mutation in a *tupGFP* background (sdc^{97}/sdc^{97}; *tupGFP/TM3*), and observed time lapse movies of dorsal vessel development. *syndecan* mutants generated similar types of defects related to cardioblast adhesion and alignment observed in *slit* and *robo,lea* mutants (Figure 8 ; Movie 8). The severity of *syndecan* phenotypes (1.55) ranked higher than wild type (0.15) and *slit* mutants (1.50), but lower than *robo,lea* mutants (2.05).

Surprisingly, despite existing defects in cardial cell organization, the rate of development in *syndecan* mutants (61 minutes for stage 15-16) was comparable to wild type animals (54 minutes for stage 15-16) (Figure 3). The speed of cardioblast migration was not found to be statistically significant ($p<0.05$) between these two groups at stages 14-17 (8.18–29.05 μm/hr, n = 18 cells, for *syndecan* mutants compared to 8.22-30.02 μm/hr, n = 18 cells, for wild type) (Figure 10; Appendix 3). However, we found migration rates to be significantly different at stage 13-14 (20.01-25.98 μm/hr, n = 6 cells for *syndecan,* compared to 22.48-34.50 μm/hr, n = 6 cells for wild type) (Figure 10; Appendix 3).

Figure 8. Dorsal vessel defects in *syndecan* mutants

Defects in *syndecan* (sdc^{97}/sdc^{97}; *tupGFP/TM3)* mutants were similar to those seen in *slit* and *robo,lea* mutants. We observed cell clumping (asterisk), gaps (~), flattening of nuclei (arrow), cells in the midline (x), failure of the lumen to close (diamond), and absence of the GFP intensity difference between *svp* and *tin*-expressing cells (compare A, B, C with Figure 2 A). (A, C) are stage 16 embryos. (B) is a stage 15 embryo. Anterior is to the upper right, posterior is to the lower left. Scale bar: 2.6 pixels = 10 micrometers.

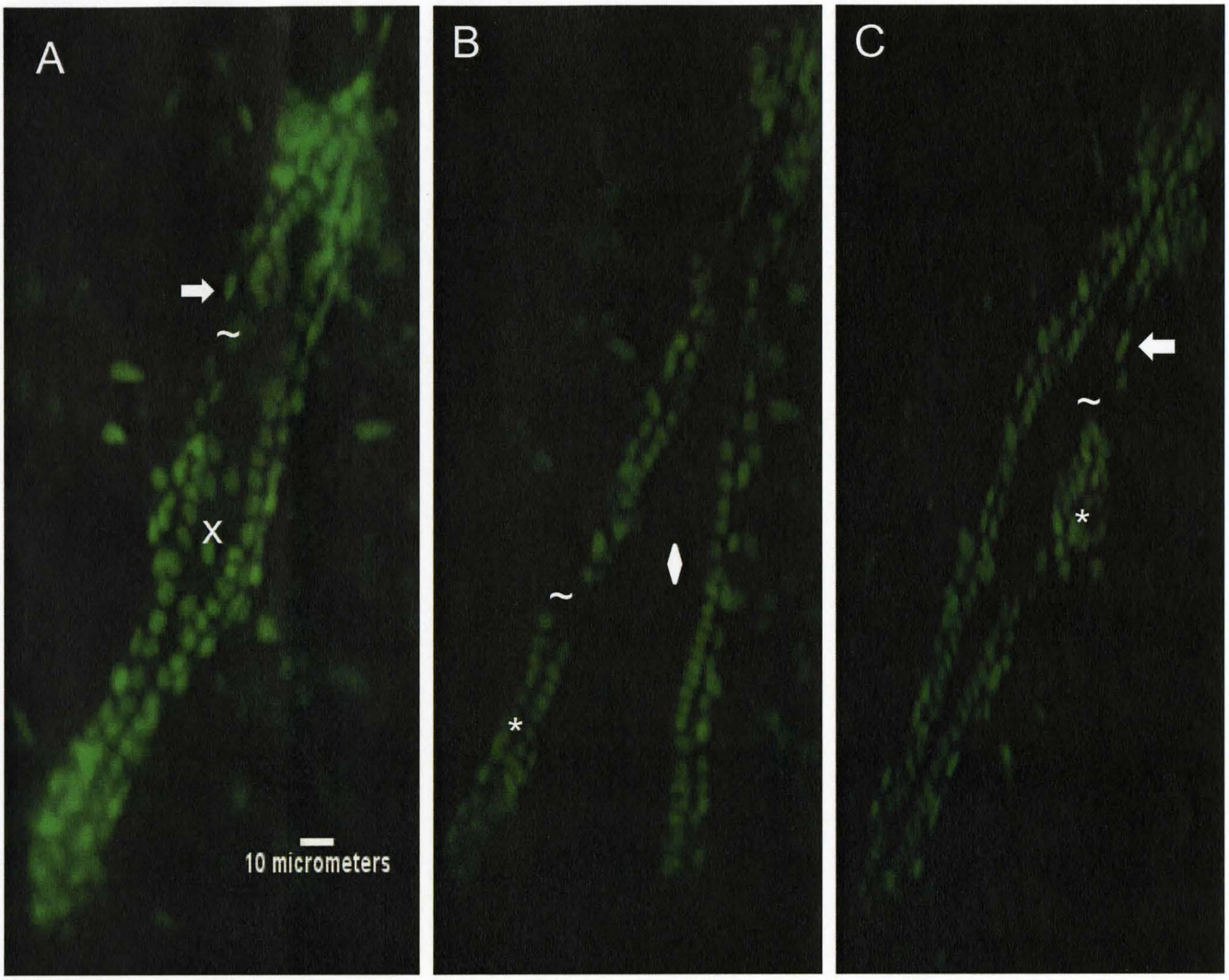
A
B
C
X
10 micrometers

3.5 Heart development in *robo,lea/syndecan* mutants

In order to gain insight into the nature of the genetic interaction between *robo, lea,* and *syndecan*, we created mutants that were triply heterozygous for these genes (*robo,lea/sdc*^{97}*;tupGFP/TM3*). We hypothesized that if these genes work in the same signaling pathway, we would see an increase in the frequency and severity of dorsal vessel defects, compared to heterozygotes for a single gene. However if these genes function in separate pathways, much milder phenotypes would be expected, since only one functional copy of each gene has been removed and the remaining copy would be sufficient for normal development.

Mutants triply heterozygous for *robo, lea* and *syndecan* resulted in the same types of defects as were observed in *slit*, and *syndecan* homozygotes and *robo,lea* double mutants (Figure 9; Movie 9), however the severity of mutant phenotypes in these embryos (0.9) was lower than in other mutants (compare to a score of 1.50 for *slit*, 1.55 for *syndecan*, and 2.05 for *robo,lea/syndecan*) (Table 1).

The rate of development in triply heterozygous embryos (63 minutes for stage 15-16), was comparable to wild type (54 minutes for stage 15-16) (Figure 3). The speed of cardioblast migration in *robo,lea/syndecan* mutants was not found to be significantly different ($p<0.05$) from wild-type for all stages (for stage 15-16, compare 17.3-19.8μm/hr, n = 6 cells to 14.6-19.9 μm/hr, n= 6 cells, respectively) (Figure 10; Appendix 3).

Figure 9. Dorsal vessel defects in *robo,lea/syndecan* mutants

As in the mutants previously examined, heart assembly defects related to cell alignment and adhesion were seen in mutants triply heterozygous for *robo, lea*, and *syndecan (robo,lea/sdc^{97};tupGFP/TM3)*. Cell clumping (asterisk), gaps (~), an absence of the GFP intensity difference between putative *svp* and *tin*-expressing cells (compare A,B,C with Figure 2 A) and cells in the midline (x) were the most commonly observed phenotypes. All embryos shown are at stage 15. Anterior is up, posterior is down. Scale bar: 2.6 pixels = 10 micrometers. Only the left side of the dorsal vessel is visible in (C) due to the position of the embryo.

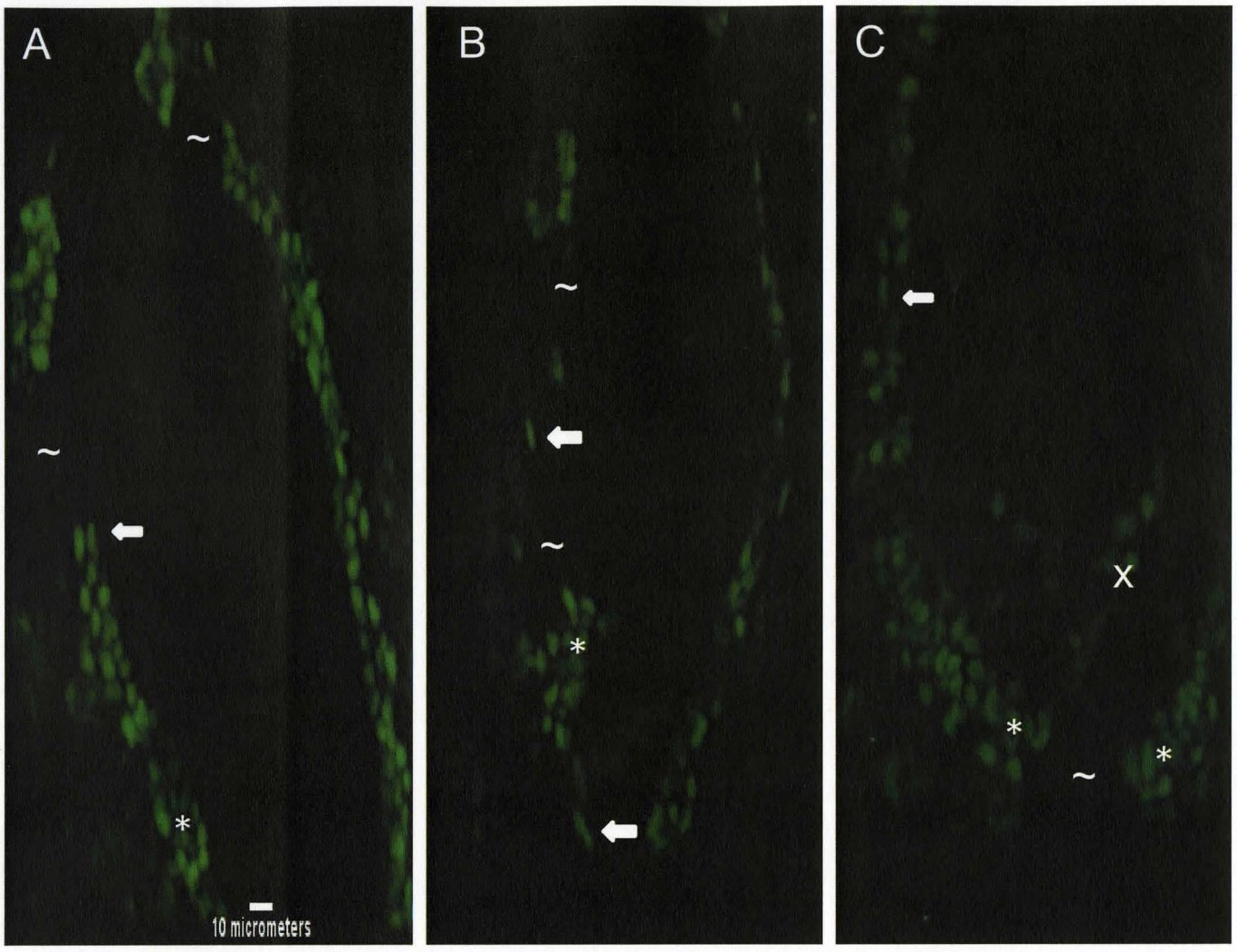
A
B
C
X
10 micrometers

3.6 Cardioblast migration speed

Repeated observations of delayed development at various stages of dorsal vessel formation in mutants (Figure 3), made us wonder if these delays were correlated with a slower speed of cardioblast migration toward the midline. In order to answer this question, we used ImageJ software to measure the distance traveled by six randomly selected individual cells within segments A2-A5 of wild type and mutant embryos over a period of 60 minutes, and at various developmental stages (Figure 10). A different embryo was used for each stage. We then applied the non-parametric, ranked sum Mann-Whitney test to the data set to see if there was a significant difference in migration speed between wild type and mutants. Migration speeds from each stage in mutant development were ranked and tested against data obtained for each stage of wild type development, except in the case of *robo,lea* mutants, where data was only available for stages 15-16 and 16-17. In this case, we only compared migration speeds for stage 15-16 and 16-17 in *robo,lea* with migration speeds for stage 15-16 and 16-17 in wild type, respectively.

Our data indicates that the cells of *robo,lea* and *robo,lea/syndecan* mutants traveled at migration speeds comparable to wild type, while *slit* mutants had cardioblast migration speeds that were significantly slower ($p<0.05$) at every stage (Figure 10; Appendix 3). Interestingly, we found that in *syndecan* mutants, the speed of migration was significantly slower than wild type at stage 13-14, but was comparable to wild type thereafter (Figure 10; Appendix 3). Despite these differences, a trend was observed in both wild type and mutant animals, where the speed of migration was faster in earlier stages of development

(13-15), and became progressively slower in later stages (15-17) (Figure 10). The slowest speeds of migration in all embryos were recorded near the end of dorsal vessel development, between stages 16-17. These results make sense if one considers the events occurring in early and late dorsal vessel development. During early development, cardioblasts need only to maintain their relative position to other cells within the cardioblast row, and travel toward the midline. Thus, there is no hindrance to the rate of migration. In late stages of development, cardioblasts come into closer vicinity of appropriate partners, and engage in more intimate interactions and signaling with contralateral cells. In addition, cardioblast cells must undergo remodeling of their shape for lumen formation. Thus, the speed of cardioblast migration is likely slowed in order to allow these important signaling and remodeling processes to occur. In addition, the entire dorsal vessel can be seen stretching through its antero-posterior axis, as if a force was pulling it in opposite directions from either end. It appears that this stretching force causes cells within the cardioblast row to migrate laterally while still maintaining their forward momentum toward the dorsal midline. This could have been another factor which resulted in a slower migration rate. Homozygous mutants for *slit* experienced especially slow rates during these last stages of development, traveling as little as 3 or 4 μm/hr (compared to over 8 μm/hr for wild type) (Figure 10).

Figure 10. Cardioblast migration speed

Plot of migration speed of cardioblasts toward the midline in *wild type* (◊), *robo,lea* (□), *slit* (Δ), *syndecan* (×), and *robo,lea/syndecan* (○) mutants at various developmental stages (13-17). Using ImageJ software, the distance of cell migration was obtained for each embryo (in pixels), by measuring the position of a particular cell at time t=0, and at t=60 min. Measurements were taken of six randomly selected cardioblast cells within segments A2-A5 of the dorsal vessel. Each distance was then multiplied by 0.387585 μm/pixel (the pixel size for the 40x objective lens used to obtain movies), to obtain a migration rate in μm/hr.

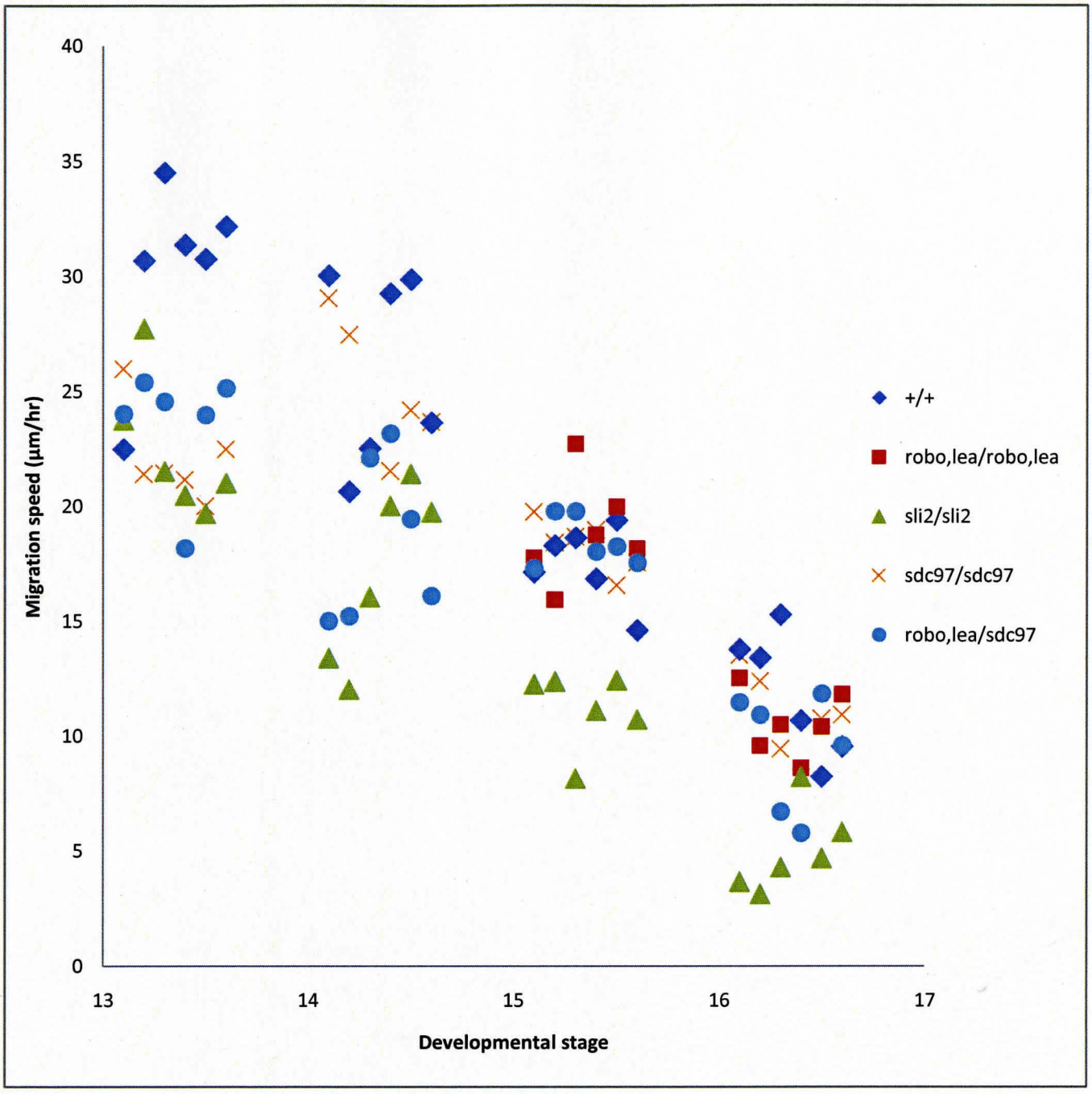
40
35
30
25
20
15
10
5
0
Migration speed (µm/hr)
13
14
15
16
17
Developmental stage
+/+
robo,lea/robo,lea
sli2/sli2
sdc97/sdc97
robo,lea/sdc97

3.7 Leading edge morphology of cardioblast cells in wild type and *slit* mutants

Observations carried out previously in our lab (MacMullin, unpublished), indicated that wild type cardioblasts develop prominent apical leading edges which reach toward the midline and their contralateral partners. These leading edges likely serve to form necessary contacts between opposing cardial cells in order to seal the heart tube and produce a lumen. The presence of these leading edges was verified during the present study (Figure 11; Movie 10). In addition to larger leading processes, multiple thin, web-like projections were observed extending from cardioblast cells toward their contralateral neighbours in wild type animals (Movie 10). These extensions did not appear to extend from one particular cell to another, but rather appeared as a network between groups of cells on either side of the dorsal midline. In contrast to wild type, *slit* mutants exhibited smaller or altogether absent apical leading edges. In some cases, when they were present, the leading edges appeared to be misdirected toward adjacent cardioblast neighbours instead of contralateral partners (Figure 11 B). In other cases, leading edges appeared to form properly on cells within one row of cardioblasts, but not on the the contralateral partner cells (Figure 11 C). The thin, web-like projections also appeared to be absent in *slit* mutants (Movie 11).

Figure 11. Leading processes in wild type and *slit* cardioblasts

In wild type cardioblasts, prominent apical leading edges (arrows) reach toward the midline and contralateral partners (A). In *slit* mutants, leading edges (arrows) adhere to adjacent rather than contralateral cells (B), or form on one side of the midline, but not the other (C). All embryos shown are stage 16-17, and express membrane-targeted *UAS CD8 GFP* which is driven by the muscle-specific *DmefGAL4* driver. Anterior is up, posterior is down. Scale bar for A-C: 5.6 pixels = 10 micrometers.

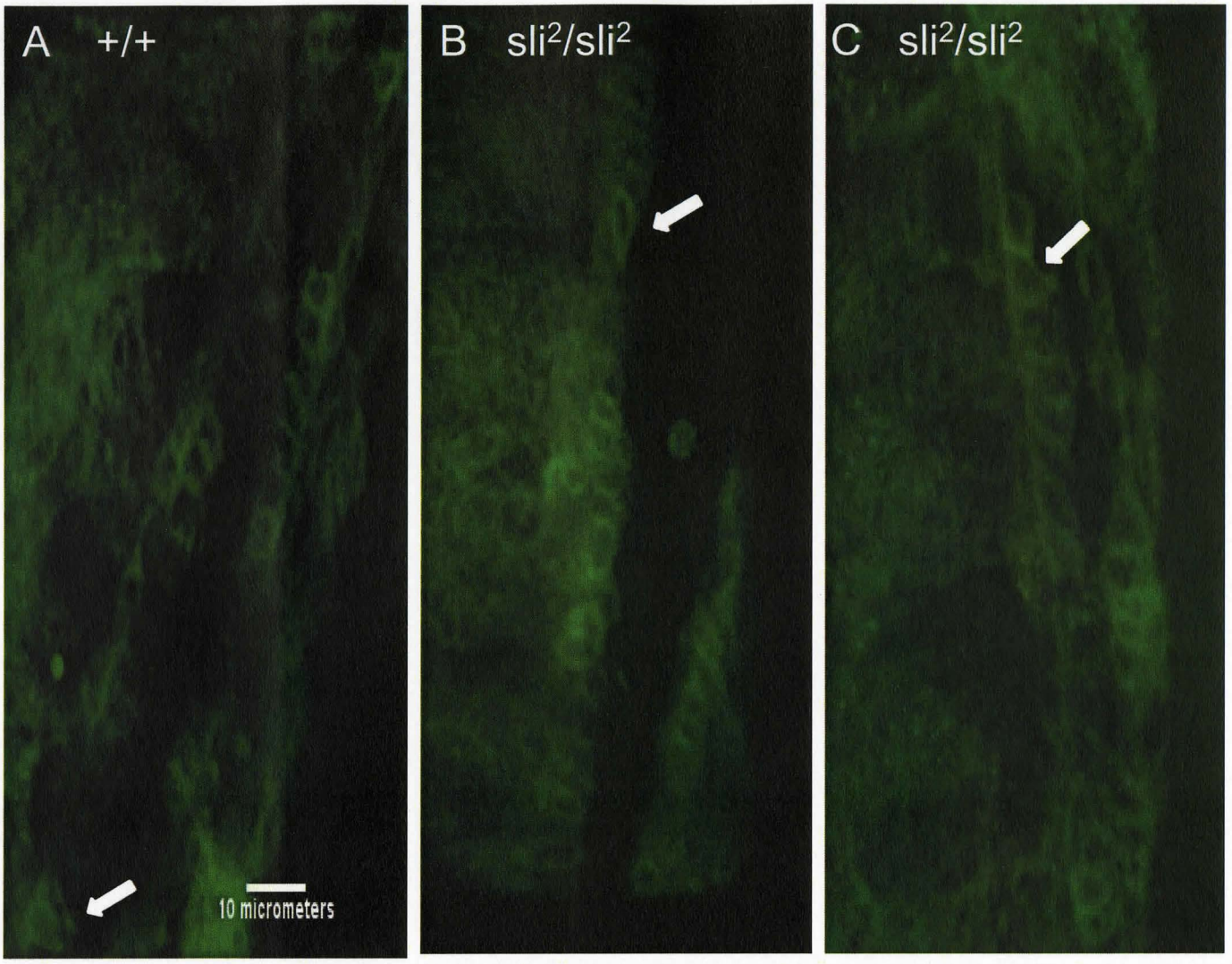
A +/+
10 micrometers
B sli2/sli2
C sli2/sli2

Chapter 4

Discussion

4.1 Functional analysis of *slit, robo, lea* and *syndecan*

In order to gain further insight into the role of *slit*, *robo*, *lea*, and *syndecan* in cardiac cell migration and dorsal vessel morphogenesis, we studied time lapse movies of heart development in embryos mutant for these genes. We observed defects associated with cell alignment, migration, and adhesion such as cell clumping, gaps within the normally continuous cardioblast cell rows, flattening of nuclei, and cells in the midline. In more severe cases, the heart was separated into multiple, separate lumens or the lumen failed to close. These observations were in accordance with the findings of others (Bodmer et al., 2005; MacMullin and Jacobs, 2006; Santiago-Martinez et al., 2006).

During wild type dorsal vessel development, cardioblast cells remain faithfully adhered to adjacent partners and move toward the midline as a continuous sheet. This adhesion and positioning of cells was disrupted in all mutants observed in this study. Interestingly, lone cells which had detached from the normally continuous cell rows were seen migrating into the midline or toward other, more ipsilaterally located cells (Figure 5). In a few cases, lone cells were successful in reaching their contralateral partner. In most cases, however, lone cells appeared to travel in a random fashion, and adhered to inappropriate cell partners. Cardioblast cells migrating alone frequently exhibited a flattened nuclear morphology (Figure 5 B). This behavior could be associated with the cell membrane changing shape and producing protrusions, perhaps as a

mechanism for searching for surrounding cells in the environment. Indeed, it was observed that once a lone cell with a flattened nuclei had met with another cell, its nuclei reverted to the same rounded appearance of cells that had not left the continuous cardioblast row (Figure 5 C). Our observations of lone cells indicate that individual cardioblasts have the ability to migrate on their own, and do not necessarily need to travel within the sheet-like cardioblast row. More importantly, the behavior of lone cells suggests their migration is not guided by an attraction to the dorsal midline.

In the current understanding of Slit as a guidance cue, Robo receptors are hypothesized to respond to a gradient of Slit protein, typically located tens or hundreds of microns away (Kramer et al., 2001; Gallio et al., 2004). During morphogenesis, guidance cues are generated by target cells in order to direct cell migration. Several systems in Drosophila employ guidance cues in such a manner during development, including the tracheal system and CNS. However, in the dorsal vessel, the Robo receptor and its ligand Slit are both expressed in the same cell (Bodmer et al., 2005; MacMullin and Jacobs, 2006). The expression of Slit and Robo, as well the behavior of lone cells characterized in this study, suggest that dorsal vessel development may not rely on repulsive or attractive guidance cues as does the developing CNS for example, where midline glial cells secrete Slit, and provide repulsive cues for the growth of axons and muscle cells (Battye et al., 1999). Thus, Slit and Robo may function in a different manner during heart morphogenesis than in the CNS or other systems.

Abnormal lumen formation was observed in all mutants in this study. The formation of a luminal defect was usually initiated by the presence of gaps (ie, missing

cells) within one or both bilateral cardioblast rows. In most cases, as long as they remained adhered to their lateral neighbours and within their rows, cardioblasts on either side of the gap proceeded to migrate normally toward the midline, and contacted appropriate contralateral partners. In this way, cardioblasts "sealed off" the normally formed portion of the lumen from the lesion, thus excluding lone or wandering cells, and leaving them without cardioblast partners (Figure 4. D; Figure 7. A,B). In some embryos, several areas with lesions resulted in lumens that were segmented into multiple parts. Another phenotype we observed was a laterally curved, twisted lumen (Movie 4,7,8). In this case, cardioblasts appeared to intercalate with contralateral partners more than normal, clumping together with their opposing neighbors and not allowing a central luminal compartment to form between them. At the same time, some cells crossed into the midline or even migrated across the midline into the opposing cell row (Figure 4. B,C; Figure 7. A,B; Figure 8. A). The effect of these cell behaviours appeared to cause it to twist and curve laterally, rather than remaining straight and centered at the midline.

Vessel formation requires the cadherin family of proteins, which carry out both adhesive and signaling functions (Dejana et al., 1999). E-cadherin is a cell junction protein specifically localized at points of cell contact (Bach et al., 1998; Vincent et al., 2004). Localization of this protein must be regulated at various parts of the cell in order to permit cell shape changes and the proper formation of a lumen. According to the mechanisms proposed by Santiago-Martinez et al. (2008) and Medioni et al. (2008), proper lumen formation depends on selective Slit/Robo signaling to inhibit E-cadherin mediated cell adhesion at different parts of contralateral cardioblasts. Slit/Robo inhibition

of E-cadherin occurs at the apical domain of cardioblasts, where apical membranes are consequently repelled from each other, resulting in the formation of a luminal space. In contrast, an absence of Slit and Robo at the dorsal and ventral points of cell contact allows the accumulation of E-cadherin, and therefore adhesion of the cells in these areas (Santiago-Martinez et al., 2008; Medioni et al., 2008). In the present study, we observed that in mutants lacking both copies of *slit*, as well as in mutants doubly mutant for *robo,lea,* contralateral cardioblasts appeared to clump together and intercalate more than normal, not allowing for the formation of a central luminal compartment which was evident in wildtype. These observations are in agreement with the proposed role of Slit and Robo in lumen formation.

In each of the mutants independently examined in this study, we observed heart assembly defects associated with cardial cell positioning, adhesion and alignment. We also observed obvious abnormalities in the formation of the heart lumen. Thus, it may be concluded that the genes *slit, robo, lea*, and *syndecan* all play a role in controlling these important processes. The fact that null mutants for *slit, robo,lea* and *syndecan* produce the same types of defects indicates that these genes may work in the same or converging signaling pathways. However, presently the nature of the genetic relationship among these genes remains unclear and will be the focus of a discussion later in this chapter.

4.2 Cardioblasts of *slit* mutants have abnormal leading edges and lack lamellipodial projections

Two types of cellular membrane projections were discernable in videos of wild type cardioblast cells. The first type of projection was filopodial in nature, producing prominent polarized apical leading edges which reached toward directly contralateral partners and the dorsal midline (Figure 11 A). The other, less apparent projections were fine and web-like, resembling lamellipodia (Movie 10). There were numerous projections of this sort across the midline. They did not appear to be directed from any one particular cell to another one particular cell, but appeared rather as a network of projections between a group of cells in close vicinity to each other. Both types of cellular extensions became visible during later stages in development (late stage 15 onward).

The classically defined functions of cellular protrusions such as lamellipodia and filopodia have been for motility (Kleitman and Johnson, 2005) and sensing the environment (Redher and Kater, 1996), respectively. The branched design of lamellipodia help direct the cell's migration and facilitate its movement across a surface by providing a stable foundation (Lee et al., 1993). In contrast, the polarized protrusions of filopodia participate in sensing the local environment for signaling cues (Cell Migration Gateway). Filopodia also likely contribute to establishing necessary cell-cell contacts (Choi and Siu, 1987). Applying this understanding of cellular extensions to cardioblasts, the lamellipodia and apical leading edges produced by filopodia may be dependent on the presence and function of one another, and may work in tandem to produce a cellular response. Perhaps the filopodia sense the environment (ie, find contralateral partners), and deliver cues to native cells, which then activate cytoskeletal rearrangement and the production of

lamellipodial extensions to initiate cell migration. Support for this hypothesized sensing and signaling mechanism comes from an observation of the cardioblast cells of *slit* mutants, where the filopodial extensions appear misdirected toward inappropriate partners (Figure 11. B), reduced in size, or completely absent (Figure 11. C), and there is a corresponding absence of web-like lamellipodia (Movie 11). In addition, *slit* mutants exhibited a significantly slower rate of cell migration than wild type (Figure 10; Appendix 3). It has been shown that *slit* mutants produce obvious heart assembly phenotypes including defects in cardioblast alignment and positioning (Bodmer et al., 2005; MacMullin and Jacobs, 2006; Santiago-Martinez et al., 2006; this study). These defects may occur in part due to the absence or abnormal formation of cell membrane extensions such as lamellipodia and filopodia, preventing a cell from being able to sense the environment, to migrate, or both.

The authors of two studies working on retinal morphogenesis in *Drosophila* described thin cellular projections, similar to the putative lamellipodia observed in our study. The cellular projections were also directed across a lumen (the eye disc lumen) (Cho et al., 2000; Gibson and Schubiger, 2000). The *Drosophila* eye disc is a single-layered sac of epithelial tissue with two opposing sides, the peripodial membrane and the disc proper. The projections, called peripodial projections, were found to originate from the peripodial membrane and run across the eye disc lumen to the opposing side - the disc proper. The secreted proteins Hedgehog, Decapentaplegic, and Wingless are expressed in the peripodial membrane, but were shown to control the dorsoventral patterning in the opposing disc proper by controlling expression of the Notch ligands, Delta and Serrate.

Cho et al. (2000) proposed two possible mechanisms for signal transmission from the peripodial membrane to cells of the disc proper. The first was that signaling molecules were secreted from peripodial membrane cells and diffused to the disc proper. Alternatively, the authors proposed that signaling molecules may be delivered across the lumen to their targets in the disc proper, via the peripodial processes which they had observed protruding from peripodial membranes. In agreement with the second proposed mechanism, Gibson and Schubiger (2000) were able to show that long-range signaling via translumenal, microtubule-based apical extensions does in fact occur in eye primordia, and was also shown to occur in wing primordia.

A more recent study on the development of thoracic mechanosensory bristles lends further support for the existence of a long-range signaling mechanism via cellular extensions (de Joussineau et al. 2003). In this study, it was shown that cells of a neural fate, which would go on to form sensory bristles, utilized cellular extensions that reached over several cell diameters to inhibit surrounding cells from adopting a similar neural fate, and forcing them to take on an epidermal identity. The mechanism of inhibition was shown to work through Notch/Delta signaling. Extensions from the neural competent cells contained Delta protein at their tips, which was delivered to the Notch receptor on target cells, by direct contact. When the authors prevented the formation of cellular projections that would normally form on neural competent cells, the ability of sensory organ precursors to signal to compatriot cells was compromised, resulting in flies with too many mechanosensory bristles (de Joussineau et al. 2003).

Robo expressing cells have typically been found tens or hundreds or microns away from the source of Slit (Kramer et al., 2001; Gallio et al., 2004), therefore it is possible that Slit is delivered to its receptors, Robo, Robo2, and/or Syndecan, via a long-range signaling mechanism similar to the one described. The thin protusions seen extending from cardioblast cell membranes may contain Slit protein at their tips, which may be delivered across the dorsal midline to contralateral partners and directly to their receptors. This proposed long-distance signaling mechanism offers a novel interpretation of Slit and Robo function which differs from the classical understanding of Slit signaling through Robo via a diffusible gradient. It is important to keep in mind, however, that an important distinction exists between the migratory cardial cells of the dorsal vessel and cells of the eye/wing discs and epithelium, which are all stationary. Similar experiments as those discussed above should be conducted in tissues known to contain migratory cell types to ascertain whether the migratory status of a cell has bearing on the effectiveness of this signaling mechanism.

While a potential role for lamellipodia has been hypothesized in long-range signaling and motility, the function of leading edge filopodia during heart morphogenesis remains unclear. MacMullin and Jacobs (2006) postulate that the formation of leading edges is characteristic of presumptive *svp* expressing cells, and that these cells are the first to reach the midline and initiate midline fusion of other migrating cardiac cells. What are the mechanisms by which these cellular protrusions develop? The Enabled (Ena)/VASP family of proteins have been proposed to aid cell-cell contacts by eliciting protrusive cell behavior of cardioblasts which allows them to touch each other

(Gates et al., 2007). Ena has been shown to affect cell motility by regulating actin dynamics. Ena/VASP promotes cell protrusion by blocking the binding of capping proteins which inhibit filament growth, thereby allowing for the elongation of actin filaments (Bear et al., 2002). Interestingly, recent work has uncovered a paradox in Ena/VASP function. Although an increase in the concentration of Ena/VASP has been shown to be correlated with a higher rate of cell protrusion (Rottner et al., 1999), it also corresponds to a decreased speed of migration in fibroblasts (Bear et al., 2000). Although its role in lumen formation is still unclear, Ena has been shown to be important for during dorsal closure (Gates et al., 2007).

Ena/VASP is not the only regulator of cellular protrusion. Protrusive cell behaviour also requires suppression of contractile signals located downstream of the small GTPase RhoA (Bass et al., 2008). This regulation has been shown to be mediated synergistically by integrins and syndecans (Bass et al., 2008). This integrin/syndecan relationship is the focus of the next discussion.

4.3 Syndecan does not affect the speed at which cardioblasts travel to the dorsal midline after stage 14

In this study, we were able to show that although null mutants for *syndecan* resulted in abnormal heart assembly phenotypes, the speed at which cardioblast cells migrated to the dorsal midline was not significantly different from wild type for stages 14-17 (Figure 10; Appendix 3). However, we did find *syndecan* mutant cardioblasts travelled significantly slower than wild type at stage 13-14 of development (Figure 10; Appendix 3). These results suggest that Syndecan plays a role in cell adhesion and

alignment throughout all stages of heart development, but only affects cell motility and speed at very early stages. In mutants triply heterozygous for *robo,lea* and *syndecan*, the speed of migration of cardioblast cells is comparable to wild type and *syndecan* homozygous mutants (Figure 10; Appendix 3). This finding lends further support for the idea that Syndecan's primary function does not affect the migration speed of cardial cells.

How does cell migration occur, and what are the possible hindrances to the speed of migration? The movement of cells along surfaces is affected by several processes, including extension and retraction of the leading edge, and cell-ECM adhesion (Lee et al., 1993). Migration is initiated when molecules such as growth factors and ECM proteins bind to cell surface receptors. The integrin family is an example of such cell surface receptors (Vandenberg, 2008). Integrins make migration possible by adhering to the ECM and activating intracellular cascades that promote actin polymerization involved in lamellipodial extension (Ridley et al., 2003; Morgan et al., 2007; Berrier and Yamada, 2007). Rac, part of the Rho family of small G proteins, is important for lamellipodial extension. Rac activation is promoted at the leading edge of cells by phosphorylation of integrins in this area, while simultaneously being inhibited at the trailing edge by integrin dephosphorylation (Ridley et al., 2003; Rose et al., 2007). In this manner, cells are able to travel across a substrate as they both adhere and release their hold on the surface (Ridley et al., 2003; Morgan et al., 2007; Berrier and Yamada, 2007). Differential regulation of signals at the leading and trailing edges is an essential aspect of cell migration, and key determinant of migration velocity (Morgan et al., 2007).

Interestingly, syndecan-4 has also been shown to affect Rac regulation (Morgan et al., 2007). Several studies have demonstrated that both receptors are necessary for the formation of focal adhesions (Woods et al., 1986; Bloom et al., 1999; Bass et al., 2008), however other studies have provided evidence that integrins alone are sufficient for focal adhesion formation (Wang et al., 2005). If the first argument is true, and both receptors are needed for the formation of focal adhesions, one would expect cell migration to be affected, and *syndecan* mutants to exhibit a slower cardial cell migration velocity. This is contrary to our data in the present study. However, it is important to keep in mind that signalling pathways can be regulated by a variety of different integrin-syndecan pairs, thus resulting in varied cellular responses (Morgan et al., 2007), therefore the particular type of interaction between syndecan and integrins during heart morphogenesis may have no effect on migration speed.

We have already shown that essential cell membrane protrusions necessary for motility and signaling are absent or abnormally formed in *slit* mutants (Figure 11; Movie 11), and that a significantly slower rate of cardioblast migration is seen in these mutants, compared to wild type (Appendix 3). However, it is unclear whether cellular filopodia and lamellipodia are solely responsible for determining cell motility and speed, or if other factors associated with cell morphology or function are involved. Time lapse observations of *syndecan* homozygous mutants expressing membrane-targeted *UAS CD8 GFP* should help answer this question. If cellular extensions are important in determining migration speed, it is expected that *syndecan* mutants would exhibit normal filopodia and lamellipodia, as in wild type. However, if migration speed relies on some other process,

one would expect to observe abnormally formed or absent filopodia and lamellipodia, as seen in *slit* mutants.

Cardioblast migration coincides with the process of dorsal closure, when ectodermal cells move and reorganize to replace the extraembryonic tissue known as the amnioserosa, and seal the dorsal part of the embryo. Throughout development of the dorsal vessel, migrating cardioblasts maintain close contact with the leading edges of the ectoderm, and rely on this association for movement (Rugendorf et al., 1994). Several heart-expressed genes are known to be required for cardioblast migration. One such gene is *pericardin* (*prc*), which encodes a collagen-like component of the ECM. Prc is expressed by the pericardial cells at the beginning of dorsal closure. However, as dorsal closure proceeds, Prc becomes concentrated at the basal surface of cardioblasts, which are in close proximity to the overlying ectoderm. In *prc* mutants, cardioblast migration and assembly is disrupted. Thus, its pattern of expression and mutant phenotype suggest that Prc mediates the coordinated migration of cardioblast rows and overlying dorsal ectodermal sheets.

The finding that Syndecan does not affect cardioblast migration speed during most stages of heart development may indicate that this gene is not expressed in an area in which it would be in a position to interact with ectodermal cell surfaces. However, this argument can be contended by the finding that in *slit* mutants, the process of dorsal closure is unaffected (MacMullin and Jacobs, 2006), even though cardioblast migration speed is significantly slower than wild type, and an overall delay in development is observed, Thus, although the relationship between ectoderm and mesoderm is important

in the morphogenesis of the dorsal vessel, there must be other mechanisms responsible for the migration of cardioblasts toward the midline. It remains to be discovered how Syndecan mediates these migratory mechanisms.

4.4 *syndecan* has a genetic interaction with genes for Robo/Robo2 receptors

In order to ascertain the nature of the genetic relationship between the receptors *syndecan, robo*, and *lea*, we applied a technique which was first used to uncover genes that participate in CNS development along with *slit* (Fritz and VanBerkum, 2002; Stevens and Jacobs, 2002), and was later adapted to screen for genes interacting with *slit* during heart morphogenesis (MacMullin and Jacobs, 2006). Although embryos homozygous for *syndecan* result in observable heart assembly defects, embryos heterozygous for one null allele of *syndecan* have a normal dorsal vessel phenotype. If the function of other genes participating in the same pathway as *syndecan* is similarly reduced, and if a genetic interaction between these genes exists, we expect to see an abnormal heart phenotype. Thus, this technique allows for the uncovering of genes that participate in the same or converging biological pathways. Applying this modifier screening technique, we constructed triply heterozygous mutants for *robo, lea* and *syndecan* (*robo,lea/sdc*^{97}*;tupGFP/TM3*), and observed dorsal vessel morphogenesis in these embryos.

The phenotype of triply heterozygous mutants was similar to the phenotypes seen in homozygous *slit* and *syndecan* mutants, as well as *robo,lea* double heterozygotes. We

observed typical cardiac assembly and alignment defects such as cell clumping, gaps, and cells in the midline, as well as abnormalities in lumen formation. The finding of a mutant phenotype indicates that there is a genetic interaction between the *syndecan, robo*, and *lea* genes. Previous dosage modifier screening carried out in our lab revealed that *syndecan* exhibited a stronger genetic interaction with *lea*, than with *robo* (Komosa, 2008).

The severity of the phenotypes seen in triply heterozygous mutants was mild compared to those observed in homozygous *slit* and *syndecan* mutants and doubly homozygous *robo,lea* mutants (Table 1). This is an expected result since triply heterozygous embryos were only mutant for one copy of each gene. Thus, the function of each gene is reduced, but not completely eliminated.

We found that the speed of cardioblast migration in *robo,lea/syndecan* mutants does not differ significantly from wild type ($p<0.05$) (Figure 10; Appendix 3). Thus, although there is a genetic interaction between the genes coding for these receptors, (as evidenced by the observable heart assembly phenotypes), the mechanism(s) which control cardioblast migration speed are not significantly affected.

4.5 Potential interactions of *slit, robo, lea*, and *syndecan*

Previous work has indicated that Syndecan, like Slit, has an integrin-dependent function in the dorsal vessel (Morgan et al., 2007 ; Komosa, 2008). Abnormal heart phenotypes were observed in mutants doubly mutant for *syndecan* and αPS3 integrin (*scb*), as well as *syndecan* and integrin ligands such as Laminin A (*lanA*), Laminin α1,2 (*wb*) and Collagen IV (*vkg*), and *syndecan* and intracellular messengers Integrin Linked Kinase (*ilk*) and Talin (*rhea*) (Komosa, 2008). These interactions were similar to those

seen in mutants heterozygous for *slit* and genes for integrins or downstream messengers (MacMullin and Jacobs, 2006), suggesting that Slit and Syndecan work through the same or converging pathways. In the present study, observed defects related to cell adhesion in the dorsal vessels of *syndecan* mutants add support for an integrin-based function of this protein. No significant genetic interaction was found between Syndecan and Robo or downstream Robo-related genes (Komosa 2008). However, a genetic interaction was seen between Syndecan and Robo2 as well as Syndecan and Ras, a downstream target of Robo2 signaling (Komosa 2008), while only a weak interaction was observed between Slit and Robo2 and Slit and Ras (MacMullin and Jacobs, 2006). In the present study, mutant phenotypes in embryos triply heterozygous for *syndecan, robo*, and *lea* also indicate the presence of a genetic interaction. Collectively, these results suggest that during dorsal vessel development, Syndecan does not signal through Robo, and may work with Slit and Robo2 individually, through two different pathways, rather than by forming a ternary complex with them, as previously suggested by Hohenester et al. (2006).

The expression pattern of Syndecan remains unknown, but could be helpful in ascertaining the role of Syndecan in lumen formation and heart morphogenesis in general. An antibody created against Syndecan would establish where this protein is localized, in comparison to Slit and Robo, and thus possibly offer insight into the functional relationship of Syndecan with these proteins. Antibodies for Slit. Robo and Robo2, if available, can be utilized in the same context. For example, as suggested by Komosa (2008), an antibody against Slit in mutants homozygous for *syndecan* can establish

whether Syndecan participates in the localization of Slit. If so, we would expect the normal localization of Slit in the lumen to be disrupted in *syndecan* mutants.

It is possible that Slit has Syndecan-dependent and Syndecan-independent functions. In this context, migration speed during stages 14-17 of heart development would be a Syndecan independent cell process. If Syndecan plays a role in the localization of Slit during lumen formation, how is Slit able to modify migration speed if it is Syndecan-independent? Based on the observations in this study, it appears that Slit participates in a signaling pathway which affects cell motility and speed during the entirety of development, while Syndecan only affects these processes very early in development. Thus, Syndecan may be stabilizing Slit at the appropriate location via its heparan sulfate chains, but not necessarily participating in signaling downstream of Slit (ie, participating in an independent pathway). Alternatively, Syndecan may be participating in the same signaling pathway as Slit during early development, but then may be involved in a different pathway during later stages of development.

4.6 Directions for future research

Using time lapse imaging in order to observe general morphology and behavior of cardiac cells is an effective tool for gaining insight into the role of specific genes involved in cardiac morphogenesis because we are able to compare how these cells behave in wild type to how they behave in animals mutant for these genes. While many labs have characterized Slit as having a repellent function (Brose et al., 1999; Kidd et al., 1999; Battye et al., 1999), it has also been shown in some cases to participate in attractive

signaling (Kidd et al., 1999; Simpson et al., 2000), and adhesion to the ECM through integrins (MacMullin and Jacobs, 2006). Clearly, Slit is a dynamic protein capable of producing more than one different cellular response.

Slit contains a variety of different domains including leucine-rich repeats at its N-terminal (known to be the binding site for Robo) (Hohenester et al., 2006), and at its C-terminal, a laminin-like G domain, and multiple EGF repeats (Rothberg et al., 1990). These C-terminal domains resemble Laminin domains, and are known to be required for adhesive cell functions such as ECM and cell surface binding (Timpl, 2000; Gersdorff 2005). Secreted Slit has a natural proteolytic cleavage site between the fifth and sixth EGF repeat (Brose et al., 1999). Cleavage at this site can produce three separate Slit proteins *in vivo*: full-length Slit, N-terminal Slit, and C-terminal Slit (Rothberg et al., 1990). C-terminal Slit, without binding to Robo, has been shown to restore midline cell architecture in the nervous system of *slit* mutants (Battye, 2003). Preliminary experiments with C-terminal Slit in the heart suggest that it may have a morphogenic function. The misexpression of C-terminal Slit in wild type animals resulted in observable phenotypic abnormalities, while misexpression in *slit* mutants resulted in a partial rescue of phenotype (Elder, 2006). However, still relatively little is understood about the contribution of the N and C-terminals of Slit during heart development. More can be learned about the roles of these domains by studying time lapse images of mutants expressing different transgenes of *slit*, in either a *slit* mutant background or by overexpressing *slit* in wild type animals. This work will have important consequences not only for determining the roles of different *slit* transgenes during heart development, but

also will help elucidate the nature of the interaction between Slit and Syndecan (since it is known Syndecan binds via its HS chains to both the N and C- terminals) (Hohenester et al., 2006).

Time lapse confocal imaging may also be used to study the genetic interaction between *slit* and other genes known to be important during cardiac morphogenesis, (such as genes coding for integrins). Since changes in the level of Slit expression generate a gradient of morphological phenotype, Slit is amenable to dosage dependent genetic screens. Drosophila deficient in one copy of *slit* are phenotypically normal. If the level of function of another gene is reduced, and that gene works in the same or converging pathway as Slit, a heart assembly defect can be observed. This can be accomplished by creating mutant strains for candidate genes (eg. integrins), in a *tupGFP* background, similarly to what I have done in the present study. These mutant strains can then be crossed to the *slit* mutant line I have created, and observed through time lapse imaging. The behavior and morphology of mutant cells may offer insight into the functional relationship between genes of interest.

Another interesting research avenue would be to elucidate whether signals are exchanged between the amnioserosa/epidermis and the heart. It is known that migrating cardial cells maintain close contact with cells of the epidermal leading edge as well as the transient extraembryonic tissue called the amnioserosa. During early dorsal closure, migrating cardial cells remain 1-2 cell diameters behind leading edge cells and the amnioserosa, but at the final stages of dorsal closure, this gap is closed and the amnioserosa is located adjacent to the heart (MacMullin and Jacobs 2006). Considering

its proximity to the heart, it is possible that the amnioserosa participates in signaling pathways which affect heart development, perhaps even aiding in the relay of signals which allow contralateral cardioblasts to recognize one another and meet at the dorsal midline. Misexpression experiments, in which *slit* transgenes are expressed in the amnioserosa, would help elucidate whether the amnioserosa participates in relaying Slit signals, or if Slit function is cell autonomous. Another approach includes "immortalizing" amnioserosa tissue using UAS-DIAP-1, an apoptosis inhibiting gene, and observing the consequences for heart development. Recent work has shown that an upregulation of apoptotic forces in amnioserosa using apoptosis-promoting GAL4 drivers cells facilitates a faster dorsal closure of the epithelium, while disruption of these apoptotic forces using an apoptosis inhibiting driver results in a delayed closure (Toyama et al., 2008). Considering the proximity of the amnioserosa to cardial cells during embryogenesis, it is likely that such manipulations would also have consequences for heart cell morphology and behavior.

References

Bach, T.L., Barsigian, C., Chalupowicz, D.G, Busler, D., Yaen, C.H. Grant, D.S., Martinez, J. 1998. VE-Cadherin mediates endothelial cell capillary tube formation in fibrin and collagen gels. *Exp. Cell Res.* 238, 324-334.

Bass, M.D., Morgan, M.R., Roach, K.A., Settleman, J., Goryachev, A.B., Humphries, M.J. 2008. p190RhoGAP is the convergence point of adhesion signals from $\alpha_5\beta_1$ integrin and syndecan-4. J. Cell Biol. 181(6):1013-1026.

Battye, R., Stevens, A., Jacobs, J.R. 1999. Axon repulsion from the midline of the *Drosophila* CNS requires *slit* function. *Development.* 126, 2475-2481.

Battye, R., Stevens, A., Perry, R.L., Jacobs, J.R. 2001. Repellent signaling by Slit requires the leucine-rich repeats. *J. Neurosci.* 21, 4290-4298.

Battye, R.A. 2003. (National Library of Canada = Bibliothèque nationale du Canada, Ottawa).

Bear, J.E., Loureiro, J.J., Libova, I., Fassler, R., Wehland, J.,Gertler, F.B. 2000. Negative regulation of fibroblast motility by Ena/VASP proteins. *Cell* 101, 717–728.

Bear, J.E., Svitkina, T.M., Krause, M., Schafer, D.A., Loureiro, J.J.,Strasser, G.A., Maly, I.V., Chaga, O.Y., Cooper, J.A., Borisy, G.G. 2002. Antagonism between Ena/VASP proteins and actin filament capping regulates fibroblast motility. *Cell* 109, 509-521.

Beauvais, D.M., Burbach, B.J., Rapraeger, A.C. 2004. The syndecan-1 ectodomain regulates $\alpha_v\beta_3$ integrin activity in human mammary carcinoma cells. *J. Cell Biol.* 167, 171-181.

Berrier, A.L., Yamada, K.M. 2007. Cell-matrix adhesion. *J. Cell Physio.* 213, 565-573.

Bier, E. and Bodmer, R. 2004. *Drosophila*, an emerging model for cardiac disease. *Gene* 342, 1-11.

Bloom, L., Ingham, K.C., Hynes, R.O. 1999. Fibronectin regulates assembly of actin filaments and focal contacts in cultured cells via the heparin-binding site in repeat III13. *Mol. Biol. Cell.* 10, 1521-1536.

Bodmer, R. 1995. Heart development in *Drosophila* and its relationship to vertebrate systems. *Trends Cardiovasc. Med.* 5, 21-27.

Bour, B.A., O'Brien, M.A., Lockwood, W.L., Goldstein, E.S., Bodmer, R., Taghert, P.H., Abmayr, S.M., Nguyen, H.T. 1995. *Drosophila* MEF2, a transcription factor that is essential for myogenesis. *Genes Dev.* 9, 730-741.

Brose, K., Bland, K.S., Wang, K.H., Arnott, D., Henzel, W., Goodman, C.S., Tessier-Lavigne, M., Kidd, T. 1999. Evolutionary conservation of the repulsive guidance function of Slit proteins and their interactions with Robo receptors. *Cell.* 96, 795-806.

Bulow, H.E., Berry, K.L., Topper, L.H., Peles, E., Hobert, O. 2002. Heparan sulphate proteoglycan-dependent induction of axon branching and axon misrouting by the Kallmann syndrome gene *kal-1*. *Proc. Natl. Acad. Sci.* 99 (9): 6346-6351.

Bulow, H.E., and Hobert, O. 2004. Differential sulfations and epimerization define heparin sulphate specificity in nervous system development. *Neuron.* 41 (5): 723-736.

Cell Migration Gateway. Cell Migration Consortium. Primer on cell migration. *http://www.cellmigration.org/science/index.shtml* Accessed October 2008.

Chen, J.N. and Fishmann, M.C. 2000. Genetics of heart development. *Trends Genet.* 16(9):383-388

Cho, K., Chern, J., Izaddoost, S., Choi, K. 2000. Novel signaling from the peripodial membrane is essential for eye disc patterning in *Drosophila. Cell.* 103: 331-342.

Choi, A.H., Sui., C.H. 1987. Filopodia are enriched in a cell cohesion molecule of Mr 80, 000 and participate in cell-cell contact formation in *Dictyostelium discoideum. J. Cell Biol.* 104, 1375-1387.

Couchman, J.R. 2003. Syndecans: proteoglycan regulators of cell-surface microdomains? *Nat. Rev. Mol. Cell. Biol.* 4 (12): 926-937

Crossley, A.C. 1985. Nephrocytes and pericardial cells. In: Kerkut G.A., Gilbert, L.I. (eds) Comprehensive insect physiology, biochemistry, and pharmacology. Vol. 3. Pergamon Press, Oxford.

Davis, G.E., Black, S.M., Bayless, K.J., 2000. Capillary morphogenesis during human endothelial cell invasion of three-dimensional collagen matrices. *In Vitro Cell. Dev. Biol. Anim.* 36:513-519.

Dejana, E., Bazzoni, G., Lampugnani, M.G. 1999. Vascular endothelial (VE)-cadherin: only an intercellular glue? *Exp. Cell Res.* 252, 13-19.

De Joussineau, C., Soule, J., Martin, M., Anguille, C., Montcourrier, P., Alexandre, D. 2003. Delta-promoted filopodia mediate long-range lateral inhibition in Drosophila. *Nature* 426: 555-559.

Elder, C. 2006. The morphogenetic function of C-terminal Slit in the *Drosophila* heart. B.Sc. Thesis. McMaster University. 1-49.

Fishman, M.C., Olson, E.N. 1998. Parsing the heart: genetic modules for organ assembly. *Cell.* 91:153-156.
Fritz, J.L., VanBerkum, M.F., 2002. Regulation of rho family GTPases is required to prevent axons from crossing the midline. Dev. Biol. 252, 46-58.

Gajewski, K., Choi, C., Kim, Y., Schulz, R. 2000. Genetically distinct cardial cells within the *Drosophila* heart. *Genesis*. 28:36-43.

Gallio, M., Englund, C., Kylsten, P., Samakovlis, C. 2004. Rhomboid 3 orchestrates Slit-independent repulsion of tracheal branches at the CNS midline. *Development.* 131: 3605-3614.

Gersdorff, N., Kohfeldt, E., Sasaki, T., Timpl, R., Miosge, N. 2005. Laminin γ3 chain binds to Nidogen and is located in murine basement membranes. *J. Biol. Chem.* 280(23): 22146-22143.

Gibson, M.C., and Schubiger, G. 2000. Peripodial cells regulate proliferation and patterning of *Drosophila* imaginal discs. *Cell.* 103: 343-350.

Hagg, T.A., Haag, N.P., Lekven, A.C., Hartenstein, V. 1999. The role of cell adhesion molecules in Drosophila heart morphogenesis: faint sausage, shotgun/DE-cadherin, and laminin A are required for discrete stages in heart development. *Dev. Biol.* 208:56-69.

Hartenstein, V., and Mandal, L. 2006. The blood/vascular system in a phylogenetic prospective. *Bioessays.* 28:1203-1210.

Harvey, R.P. 1996. NK-2 homeobox genes and heart development. *Dev. Biol.* 178:203-216.

Hoffman, J.I. 1995. Incidence of congenital heart disease: II. Prenatal incidence. *Pediatr Cardiol* 16:155-165.

Hoffman J.I. 2004. Prevelance of congenital heart disease. *Am Heart J.* 147:425-439.

Hohenester, E., Hussain, S.A, Howitt, J.A. 2006. Interaction of the guidance molecule Slit with cellular receptors. *Biochem Soc Trans.* 34(3), 418-421.

Humphries, J.D., Byron, A., Humphries, M.J. 2006. Integrin ligands at a glance. *J.Cell Sci.* 119, 3901-3903.

Hussain, S.A., Piper, M., Fukuhara, N., Strochlic, L., Cho, G., Howitt, J.A., Ahmed, Y., Powell, A.K., Turnbull, J.E., Holt, C.E., Hohenester, E. 2006. A molecular mechanism for the heparan sulphate dependence of Slit-Robo signaling. *J. Biol. Chem.* 281(50), 39693-39698.

Inatani, M., Irie, F., Plump, A.S., Tessier-Lavigne, M., Yamaguchi, Y. 2003. Mammalian brain morphogenesis and midline axon guidance require heparin sulfate. *Science.* 302, 1044-1046.

Johnson, K.G., Ghose, A., Epstein, E., Lincecum, J., O'Connor, M.B., Van Vactor, D. 2004. Axonal heparan sulfate proteoglycans regulate the distribution and efficiency of the repellant Slit during midline axon guidance. *Curr. Biol.* 14(6): 488-504.
Kidd, T., Bland, K., Goodman, C.S. 1999. Slit is the midline repellant for the Robo receptor in *Drosophila. Cell* 96, 785-794.

Kleitman, N., Johnson. M.I. 2005. Rapid growth cone translocation on laminin is supported by lamellipodial not filopodial structures. *Cell Motility and the Cytoskeleton.* 13(4): 288-300.

Komosa, M. 2008. Heparan sulfate proteoglycan Syndecan mediates Slit signaling in Drosophila dorsal vessel morphogenesis. B.Sc. Thesis. McMaster University. 1-60.

Kramer, S.G., Kidd, T., Simpson, J.H., Goodman, C.S. 2001. Switching repulsion to attraction: changing responses to Slit during transition in mesoderm migration. *Science.* 292:737-740.

Lilly, B., Zhao, B., Ranganayakulu, G., Paterson, B.M., Schulz, R.A., Olson, E.N. 1995. Requirement of MADS domain transcription factor D-MEF2 for muscle formation in *Drosophila. Science.* 267: 688-693.

Lee, J., Ishihara, A., Jacobson, K. 1993. How do cells move along surfaces? *Trends Cell Biol.* 3(11): 366-370.

Lee, J.S., von der Hardt, S., Rusch, M.A., Stringer, S.E., Stickney, H.L., Talbot, W.S., Geisler, R., Nusslein-Volhard, C., Selleck, S.B., Chien, C.B., Roehl, H. 2004. Axon sorting in the optic tract required HSPG synthesis by *ext2 (dackel)* and *extl3 (boxer).* *Neuron.* 44(6): 947-960.

MacMullin, A. and Jacobs, J. 2006. Slit coordinates cardiac morphogenesis in *Drosophila. Dev. Biol.* 291: 154-164.

McQuade, K.J., Beavais, D.M., Burbach, B.J., Rapraeger, A.C. 2006. Syndecan-1 regulates $\alpha_v\beta_5$ integrin activity in B82L fibroblasts. *J. Cell Sci.* 119, 2445-2456.

Medioni, C., Astier, M., Zmojdzian, M., Jagla, K., Semeriva, M. 2008. Genetic control of cell morphogenesis during *Drosophila melanogaster* cardiac tube formation. *J. Cell Biol.* 182(2): 249-261

Milán, M., Weihe, U., Perez, L., Cohen,S.M. 2001. The LRR proteins capricious and Tartan mediate cell interactions during DV boundary formation in the *Drosophila* wing. *Cell.* 106:785-794.

Mitra, S.K., Hanson, D.A., Schlaepfer, D.D. 2005. Focal adhesion kinase: in command and control of cell motility. Nat Rev. 6, 56-69.

Monier, B., Tevy, F., Perrin, L., Capovilla, M., Semeriva, M. 2007. Downstream of homeotic genes: in the heart of Hox function. *Fly.* 1:59-67.

Morgan, M.R., Humphries, M.J., Bass, M.D. 2007. Synergistic control of cell adhesion by integrins and syndecans. *Nat. Rev.* 8, 957-969.
Rhiner, C., Gysi, S., Frohli, E., Hengartner, M.O., Hajnal, A. 2005. Syndecan regulates cell migration and axon guidance in *C. elegans*. *Development.* 132, 4621-4633.

Redher, V., Kater. S.B. 1996. Filopodia on neuronal growth cones: multifunctional structures with sensory and motor capabilities. *Sem. In Neurosci.* 8(2): 81-88.

Ridley, A.J. Cell migration: integrating signals from front to back. 2003. *Science* 302, 1704-1709.

Rose, D.M., Alon, R., Ginsberg, M.H. 2007. Integrin modulation and signaling in leukocyte adhesion and migration. *Immuno Rev.* 218, 126-134.

Rothberg, J.M., Jacobs, J.R., Goodman, C.S., Artavanis-Tsakonas, S. 1990. Slit: an extracellular protein necessary for development of midline glia and commissural axon pathways contains both EGF and LRR domains. *Genes Dev.* 4:2169-2187.

Rottner, K., Behrendt, B., Small, J.V. and Wehland, J. 1999. VASP dynamics during lamellipodia protrusion. *Nat. Cell Biol.* 1, 321–322.

Rugendorff, A., Younossi-Hartenstein, A., Hartenstein, V. 1994. Embryonic origin and differentiation of the *Drosophila* heart. *Roux's Arch Dev Biol.* 203:266-280.

Santiago-Martinez, E., Soplop, N.H., Kramer, S.G. 2006. Lateral positioning at the dorsal midline: Slit and Roundabout receptors guide Drosophila heart migration. *Proc. Natl. Acad. Sci.* USA. 103:12441-12446.

Santiago-Martinez, E., Soplop, N.H., Patel, R., Kramer, S.G. 2008. Repulsion by Slit and Roundabout prevents Shotgun/E-cadherin-mediated cell adhesion during *Drosophila* heart tube lumen formation. *J. Cell Biol.* 182(2): 241-248.

Simpson, J.H., Kidd, T., Bland, K.S., Goodman, C.S. 2000. Short-range and long-range guidance by Slit and its Robo receptors: Robo and Robo2 play distinct roles in midline guidance. *Neuron.* 28:753-766.

Steigemann, P., Molitor, A., Fellert, S., Jackle, H., Vorbruggen, G. 2004. Heparan sulfate proteoglycan Syndecan promotes axonal and myotube guidance by Slit/Robo signaling. *Curr Biol.* 14(3): 225-230.

Stevens, A.L., Jacobs, J.R. 2002. Integrins regulate responsiveness to Slit repellent signals. J. Neurosci. 22, 4448-4455.

Tao, Y. and Schulz, R.A. 2007. Heart development in *Drosophila. Semin. Cell Dev. Biol.* 18, 3-15.

Toyama, Y., Peralta, X.G., Wells, A.R., Kiehart, D.P., Edwards, G.S. 2008. Apoptotic force and tissue dynamics during *Drosophila* embryogenesis. *Science.* 321, 1683-1686.

Timpl, R., Tisi, D., Talts, J.F., Andac, Z., Saaki, T., Hohenester, E. 2000. Structure and function of laminin LG modules. *Matrix Biol.* 19: 309-317.
Vandenberg, C.A. Integrins step up the pace of cell migration through polyamines and potassium channels. 2008 PNAS. 105(20): 7109-7110.

Vincent, P.A., Xiao, K., Buckley, K.M., Kowalczyk, A.P. 2004. VE-cadherin: adhesion at arm's length. *Am. J. Physiol. Cell Physiol.* 286, C987-C997.

Wang, R., Clark, R.A., Mosher, D.F., Ren, X.D. 2005. Fibronectin's central cell binding domain supports focal adhesion formation and Rho signal transduction. *J. Biol. Chem.* 280, 28803-28810.

Whiteford, J.R., Couchman, J.R. 2006. A conserved NXIP motif is required for cell adhesion properties of the syndecan-4 ectodomain. *J. Biol. Chem.* 281, 32156-32163.

Woods, A., Couchman, J., Johansson, S., Hook, M. 1986. Adhesion and cytoskeletal organization of fibroblasts in response to fibronectin fragments. *EMBO J.* 5:665-670.

Yarnitzky, T., Volk, T. 1995. Laminin is required for heart, somatic muscles, and gut development in the *Drosophila* embryo. *Dev. Biol.* 169:609-618.

Zaffran, S., and Frasch, M. 2002. Early signals in cardiac development. *Circ. Res.* 91:457-469.

List of Appendices

Appendix 1. Genetic schemes for constructing mutant strains

Mutant strains for *slit, robo,lea*, and *syndecan* were constructed in a *tupGFP* background. A *GFP*-marked balancer was introduced into mutant strains in order to facilitate identification of homozygous embryos (embryos expressing the *GFP* marker were heterozygous and therefore not selected for experiments).

Step 1:

Gla/CyO$_{GFP}$ x tupGFP/tupGFP

↓

+/CyO$_{GFP}$; tupGFP/+ or *Gla/+; +/tupGFP*

Step 2:

sli^2/CyO x Sp/CyO; Ly/TM3

↓

sli^2/CyO; +/TM3 or *sli^2/Sp; +/TM3* or *sli^2/Sp; Ly/+* or *Sp/CyO; Ly/+ or sli^2/CyO; Ly/+* or *sli^2/Sp; +/TM3*

Step 3:

+/CyO$_{GFP}$; tupGFP/+ x Sli^2/CyO; +/TM3

↓

sli^2/CyO$_{GFP}$; tupGFP/TM3

robo,lea/CyO$_{GFP}$; tupGFP/TM3 and sdc^{97}/CyO$_{GFP}$; tupGFP/TM3 were constructed using the same scheme, except with *robo,lea/CyO* and *sdc^{97}/CyO,* respectively, instead of *sli^2/CyO* in step 2.

Mutants triply heterozygous for *robo,lea* and *syndecan* were obtained by crossing *robo,lea/CyO$_{GFP}$; tupGFP/TM3* with *sdc^{97}/CyO$_{GFP}$; tupGFP/TM3*

Appendix 2. Genetic scheme for constructing strains to study leading processes of cardioblasts

The strain *sli*^{2}*/CyO*$_{GFP}$*; DMefGAL4/TM3* was created during this study, and crossed to a strain previously created by Allison MacMullin (Step 4), in a house to produce embryos of three different genotypes. Embryos from (A) were used to study leading processes in wild type, while embryos from (B) were used to study leading processes in *slit* mutants. Mutants were distinguished from wild type animals by an absence of a GFP marked balancer.

Step 1:

Gla/CyO$_{GFP}$ *x DMefGAL4/DMefGAL4*

↓

+/CyO$_{GFP}$ *; DMefGAL4/+* or *Gla/+; +/DMefGAL4*

Step 2:

sli^2*/CyO*$_{(en\ lacz)}$ *x Sp/CyO; Ly/TM3*

↓

sli^2*/CyO; +/TM3* or *sli*^{2}*/Sp; +/TM3* or *sli*^{2}*/Sp; Ly/+* or *Sp/CyO*$_{(en\ lacz)}$*; Ly/+ or sli*^{2}*/CyO; Ly/+* or *sli*^{2}*/Sp; +/TM3*

Step 3:

sli^2*/CyO; +/TM3 x +/CyO*$_{GFP}$ *; DMefGAL4/+*

↓

sli^2*/CyO*$_{GFP}$*; DMefGAL4/TM3*

Step4:

yw; sli^2,UAS CD8 GFP/CyO$_{lacz}$ x yw; sli^2/CyO$_{GFPz}$; DMefGAL4/TM3

↓

A. *yw; sli^2,UAS CD8 GFP/CyO$_{GFP}$; DMefGAL4/ +*

or

B. *yw; sli^2,UAS CD8 GFP/sli^2 ; DMefGAL4/ +*

or

C. *yw; sli^2/CyO$_{lacz}$; DMefGAL4/ +*

Appendix 3. Results of Mann-Whitney statistical tests

Migration speeds of cardioblasts (in μm/hr) were obtained for each stage of development for wild type and mutant animals. Six randomly selected cells in segments A2-A5 were measured at each stage (see table below). When applying the Mann-Whitney test, we compared data for each stage of wild type development to each stage of development in mutants, except in *robo,lea*, mutants, where data was only available for stages 15-16 and 16-17. In this case, when applying the statistical test, we compared the data for stages 15-16 and 16-17 of *robo,lea* with stages 15-16 amd 16-17 of wild type only.

WT	slit	robo,lea	syndecan	robo,lea/syndecan
22.48	23.76		22.48	24.02
30.67	27.72		21.41	25.39
34.50	21.53		21.44	24.55
31.36	20.48		25.98	18.17
30.74	19.69		20.01	23.97
32.16	20.01		21.16	25.13
30.02	13.39		29.05	14.00
20.63	12.03		27.45	14.21
22.51	16.05		22.26	21.09
29.24	20.02		21.53	21.16
29.85	21.41		24.18	17.44
23.63	19.74		23.66	14.09
17.12	12.25	17.75	18.96	18.02
18.28	12.37	15.93	17.55	17.53
18.62	8.15	22.71	18.67	19.77
16.83	11.10	18.75	19.76	17.29
19.38	12.42	19.98	16.56	18.24
14.59	10.72	18.16	18.41	19.78
13.76	3.65	12.52	13.52	11.45
13.39	3.12	9.57	12.38	10.91
15.27	4.28	10.49	9.43	6.69
10.66	8.22	8.60	8.18	5.76
8.22	4.68	10.40	10.75	11.83
9.53	5.82	11.81	10.92	9.57

Mann-Whitney Test and CI: WT st. 13-14, Slit st. 13-14

```
                N  Median
WT st. 13-14    6  31.050
Slit st. 13-14  6  21.005


Point estimate for ETA1-ETA2 is 10.010
95.5 Percent CI for ETA1-ETA2 is (2.789,12.148)
W = 55.0
Test of ETA1 = ETA2 vs ETA1 not = ETA2 is significant at 0.0131
```

Mann-Whitney Test and CI: WT st. 13-14, Sdc st. 13-14

```
               N  Median
WT st. 13-14   6  31.050
Sdc st. 13-14  6  21.425


Point estimate for ETA1-ETA2 is 9.420
95.5 Percent CI for ETA1-ETA2 is (2.471,12.020)
W = 55.5
Test of ETA1 = ETA2 vs ETA1 not = ETA2 is significant at 0.0104
The test is significant at 0.0103 (adjusted for ties)
```

Mann-Whitney Test and CI: WT st. 13-14, robo,lea/sdc st. 13-14

```
                        N  Median
WT st. 13-14            6  31.050
robo,lea/sdc st. 13-14  6  24.285


Point estimate for ETA1-ETA2 is 6.770
95.5 Percent CI for ETA1-ETA2 is (4.312,10.529)
W = 52.0
Test of ETA1 = ETA2 vs ETA1 not = ETA2 is significant at 0.0453
```

Mann-Whitney Test and CI: WT st. 14-15, Slit st. 14-15

```
                N  Median
WT st. 14-15    6  26.435
Slit st. 14-15  6  17.895


Point estimate for ETA1-ETA2 is 9.170
95.5 Percent CI for ETA1-ETA2 is (2.491,15.853)
W = 56.0
Test of ETA1 = ETA2 vs ETA1 not = ETA2 is significant at 0.0082
```

Mann-Whitney Test and CI: WT st. 14-15, Sdc st. 14-15

```
                N  Median
WT st. 14-15    6  26.435
Sdc st. 14-15   6  23.920


Point estimate for ETA1-ETA2 is 0.975
95.5 Percent CI for ETA1-ETA2 is (-3.819,6.982)
W = 43.0
Test of ETA1 = ETA2 vs ETA1 not = ETA2 is significant at 0.5752
```

Mann-Whitney Test and CI: WT st. 14-15, robo,lea/sdc st. 14-15

```
                          N  Median
WT st. 14-15              6  26.435
robo,lea/sdc st. 14-15    6  17.825


Point estimate for ETA1-ETA2 is 8.725
95.5 Percent CI for ETA1-ETA2 is (2.543,15.641)
W = 55.0
Test of ETA1 = ETA2 vs ETA1 not = ETA2 is significant at 0.0531
```

Mann-Whitney Test and CI: WT st. 15-16, Slit st. 15-16

```
                N  Median
WT st. 15-16    6  17.700
Slit st. 15-16  6  11.675


Point estimate for ETA1-ETA2 is 6.225
95.5 Percent CI for ETA1-ETA2 is (4.409,8.661)
W = 57.0
Test of ETA1 = ETA2 vs ETA1 not = ETA2 is significant at 0.0051
```

Mann-Whitney Test and CI: WT st. 15-16, robo,lea st. 15-16

```
                    N  Median
WT st. 15-16        6  17.700
robo,lea st. 15-16  6  18.455


Point estimate for ETA1-ETA2 is -1.185
95.5 Percent CI for ETA1-ETA2 is (-4.160,1.190)
W = 33.0
Test of ETA1 = ETA2 vs ETA1 not = ETA2 is significant at 0.3785
```

Mann-Whitney Test and CI: WT st. 15-16, sdc st. 15-16

```
               N  Median
WT st. 15-16   6  17.700
sdc st. 15-16  6  18.540


Point estimate for ETA1-ETA2 is -0.555
95.5 Percent CI for ETA1-ETA2 is (-2.929,0.971)
W = 33.0
Test of ETA1 = ETA2 vs ETA1 not = ETA2 is significant at 0.3785
```

Mann-Whitney Test and CI: WT st. 15-16, robo,lea/sdc st. 15-16

```
                         N  Median
WT st. 15-16             6  17.700
robo,lea/sdc st. 15-16   6  18.130


Point estimate for ETA1-ETA2 is -0.800
95.5 Percent CI for ETA1-ETA2 is (-2.939,1.090)
W = 33.0
Test of ETA1 = ETA2 vs ETA1 not = ETA2 is significant at 0.3785
```

Mann-Whitney Test and CI: WT st. 16-17, Slit st 16-17

```
               N  Median
WT st. 16-17   6  12.025
Slit st 16-17  6   4.480


Point estimate for ETA1-ETA2 is 6.710
95.5 Percent CI for ETA1-ETA2 is (3.710,10.269)
W = 56.5
Test of ETA1 = ETA2 vs ETA1 not = ETA2 is significant at 0.0065
The test is significant at 0.0064 (adjusted for ties)
```

Mann-Whitney Test and CI: WT st. 16-17, Sdc st. 16-17

```
               N  Median
WT st. 16-17   6  12.025
Sdc st. 16-17  6  10.835


Point estimate for ETA1-ETA2 is 1.120
95.5 Percent CI for ETA1-ETA2 is (-2.699,4.349)
W = 43.Test of ETA1 = ETA2 vs ETA1 not = ETA2 is significant at 0.5752
```

Mann-Whitney Test and CI: WT st. 16-17, robo,lea st. 16-17

```
                    N  Median
WT st. 16-17        6  12.025
robo,lea st. 16-17  6  10.445


Point estimate for ETA1-ETA2 is 1.165
95.5 Percent CI for ETA1-ETA2 is (-2.180,4.781)
W = 44.0
Test of ETA1 = ETA2 vs ETA1 not = ETA2 is significant at 0.4712
```

Mann-Whitney Test and CI: WT st. 16-17, robo,lea/sdc st. 16-17

```
                        N  Median
WT st. 16-17            6  12.025
robo,lea/sdc st. 16-17  6  10.240


Point estimate for ETA1-ETA2 is 2.470
95.5 Percent CI for ETA1-ETA2 is (-1.379,6.700)
W = 46.0
Test of ETA1 = ETA2 vs ETA1 not = ETA2 is significant at 0.2980
```